INTERIM REPORT

AD. _____

AN EXPERIMENTAL TEST OF THE ACOUSTIC – GRAVITY WAVE INTERPRETATION OF TRAVELLING IONOSPHERIC DISTURBANCES.

BY

C.O. THOME

P.B. RAO

RESEARCH SUPPORTED BY

ADVANCED RESEARCH PROJECTS AGENCY

MONITORED BY

U.S. ARMY MISSILE COMMAND

PROJECT 5910-21-10039-02
CONTRACT DA-01-021-14482(Z)
ARPA ORDER NO.: 982 #MC

APRIL 1, 1967 – MARCH 31, 1968

ISSUED: MAY 1968

RAYTHEON COMPANY
SPENCER LABORATORY
BURLINGTON, MASSACHUSETTS

RAYTHEON

DISCLAIMER NOTICE

THIS DOCUMENT IS THE BEST QUALITY AVAILABLE.

COPY FURNISHED CONTAINED A SIGNIFICANT NUMBER OF PAGES WHICH DO NOT REPRODUCE LEGIBLY.

AN EXPERIMENTAL TEST OF THE ACOUSTIC-GRAVITY WAVE INTERPRETATION OF TRAVELLING IONOSPHERIC DISTURBANCES

Sponsored by the
ADVANCED RESEARCH PROJECTS AGENCY
Washington, D. C.

INTERIM REPORT

May, 1968

Period Covered 1 April 1967 through 31 March 1968

Compiled by:

RAYTHEON COMPANY
Spencer Laboratory
Burlington, Massachusetts

ARPA Order Number 982

Project Code Number: 5910-21-10039-02
Contract: DA-01-021-14482(z)
Dated: 11 April 1967
Expires: 28 February 1969

Authors:

G. D. Thome
P. B. Rao

This research was supported by the Advanced Research Projects Agency and was monitored by the U. S. Army Missile Command.

ABSTRACT

This report presents the results of simultaneous HF Doppler and UHF incoherent backscatter measurements of the travelling ionospheric disturbances observed at Arecibo (P. R.) during the summer of 1967. One of the prime objectives in conducting this series of experiments involving 3 spaced phase path sounders and the backscatter radar is to examine the gravity wave interpretation of the large scale travelling disturbances. The analysis of the observations is based upon three distinct techniques: (1) Cross-correlation analysis of the HF Doppler records for an accurate estimate of the wave velocity, (2) HF ray tracing for demonstrating the self-consistency of the HF and the incoherent backscatter data, and (3) the coupling of acoustic gravity waves to the ionospheric plasma. It is concluded from the results of the analysis that the large scale travelling ionospheric disturbances are truly a manifestation of the acoustic-gravity waves. Finally, some aspects of the analysis which will be refined in the next phase of the study are also outlined.

TABLE OF CONTENTS

Section		Page
I.	INTRODUCTION	1
II.	EXPERIMENT DESCRIPTION	2
	A. Station Geometry	2
	B. Equipment Characteristics	2
	1. HF Sounder Network	2
	2. Incoherent Backscatter Facility	4
III.	OBSERVATIONS	5
	A. Data Collection	5
	B. Data Reduction	5
	C. Results	5
	1. Summary	5
	2. Examples	8
IV.	ANALYSIS	15
V.	CONCLUSIONS	23
VI.	APPENDIXES	24
	A. Cross-Correlation	24
	B. Ray Tracing	28
	C. Wave Interaction with Plasma	33
	REFERENCES	41
	ACKNOWLEDGEMENTS	42

LIST OF ILLUSTRATIONS

Figure		Page
1.	The Geometry of the HF Phase Path Sounder Network	3
2.	Doppler Shift Records at the Three Sites on June 12, 1967 Using an Operating Frequency of 5.228 MHz	9
3.	Contours of Constant Plasma Frequencies from Incoherent Backscatter Measurements at 430 MHz on June 12, 1967	10
4.	Doppler Shift Recordings on June 14, 1967 at an Operating Frequency of 6.843 MHz	11
5.	Doppler Shift Recordings on July 8, 1967 at an Operating Frequency of 5.328 MHz	13
6.	Contours of Constant Plasma Frequencies from the Backscatter Measurements on July 8, 1967	14
7.	One-bit Digitized Version of the Doppler Shift Signatures of June 12, 1967	16
8.	Cross Correlograms for the 3 Pairs of Stations for a Selected 20 Minute Window Centered on the Main Signature of the Digitized Doppler Record.	17
9.	Observed and Synthesized HF Doppler Signatures of June 12, 1967	18
10.	Comparison of Variations in 5.228 MHz Reflection Level with the HF Signature at the Same Frequency at Arecibo	20
11.	Predicted Variation of the Phase of an Acoustic Gravity Wave with Altitude	21
12.	Comparison of Predicted and Observed Phase Variation with Altitude	22
13.	Cross-Correlograms for Six Successive Positions of a 20 Minute Running Window in the Test Interval 14:08:30 - 14:53:30 U.T. on June 12, 1967	26
14.	Geometrical Interpretation of the Interpolation Method	29
15.	A Representation for Typical Electron Density Cells	29
16.	Illustration for Coordinate System Transformation	31
17.	The Neutral Gas Velocity and the Geomagnetic Field Configuration	36

SECTION I. INTRODUCTION

This report is concerned with the question, "Are travelling ionospheric disturbances acoustic - gravity waves or are they not?" The development of acoustic - gravity wave theory in recent years has made it clear that if meaningful comparisons between theory and observation are to be made, the velocity, period, and vertical structure of the disturbances must be measured simultaneously.[1] HF radar measurements over the past 20 years have shown that wave periods from a few minutes to a few hours and propagation velocities from less than 100 to more than 1000 meters per second can be expected.[2] All these can be explained as acoustic gravity waves if suitable assumptions about the vertical structure are made.[1] Similarly, the period and vertical structure of a few travelling disturbances have been measured by means of incoherent backscatter[3] and these observations are consistent with the predictions of acoustic - gravity wave theory so long as suitable velocities are assumed.[4]

In this report a series of experiments is described in which simultaneous HF radar and incoherent backscatter observations of travelling ionospheric disturbances are made and the need for assuming various wave parameters eliminated.

The report begins with a discussion of the factors which influenced the experiment design, followed by a brief description of the equipment involved. The observations are then summarized and selected pieces of experimental data are shown. An outstanding example of a travelling ionospheric disturbance is selected and analyzed in detail. Finally, conclusions are drawn and the work planned for the final phase of this study is outlined.

SECTION II. EXPERIMENT DESCRIPTION

A. Station Geometry

The experiment was designed to study what are commonly called "large scale" travelling ionospheric disturbances. Typically these events have time scales of 10-30 minutes and propagation velocities on the order of 100 meters per second. They occur at the rate of about one per day and cause electron density perturbations of perhaps 10 percent. Shorter period disturbances (a few minutes) occur more frequently but cause much smaller density perturbations and therefore are difficult to study with incoherent backscatter. Longer period disturbances (a few hours) cause much larger density perturbations but occur infrequently, perhaps once a month. In view of the competition for observing time at incoherent backscatter facilities, the very small probability of occurrence for these long period events makes their study impractical.

The horizontal velocity of propagation is measured by spacing three identical HF sounders on the island of Puerto Rico and measuring time delay between the appearance of the disturbance at each station. The spacing between sounders is a compromise. The spacing must be large enough so that significant time delays will be observed but close enough so that the waveform of the disturbance will not change appreciably from station to station. Experimenters in the past have found a spacing of 30-50 km near optimum for disturbances of the time scale being sought here.[5] Convenient locations were found at the Arecibo Ionospheric Observatory where the incoherent backscatter observations were made, near Mayaguez where Prof. Braulio Dueno maintains a radio field station, and at the Ramey Air Force Base. The geometry of network is shown in Figure 1.

B. Equipment Characteristics

1. HF Sounder Network

Each of the three HF sounder installations consisted of two phase-coherent pulse radars which could be operated throughout the 3-30 MHz band. In practice the radar frequencies were chosen to lie below the vertical incidence critical frequency and all three sounders were operated on the same pair of frequencies. A pulse width of 200 microseconds, a pulse repetition frequency 20 pps, and a peak

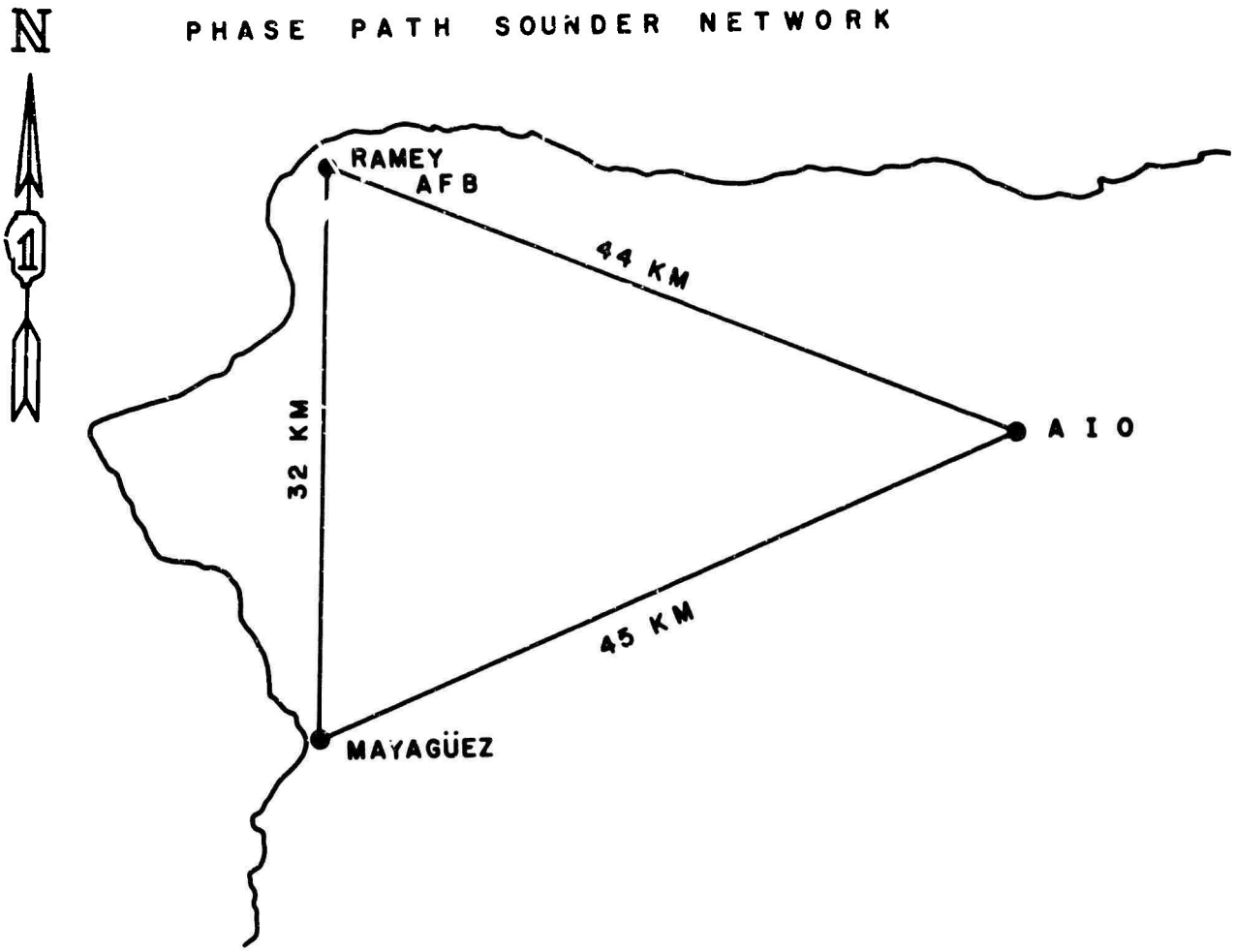

Figure 1. The Geometry of the HF Phase Path Sounder Network

pulse power of 20 kw were used at each site. The transmitted frequencies, the receiver local oscillator frequencies, and the timing circuitry were controlled from a stable master oscillator. The master oscillators at all sites were synchronized to avoid interference between stations. The receiver output was beat to a 5 cps IF and recorded on analog mangetic tape. The tapes were mailed to the Raytheon laboratories at Burlington, Massachusetts for spectrum analysis.

2. Incoherent Backscatter Facility

The incoherent backscatter observations were made using the 430 MHz radar at the Arecibo Ionospheric Observatory. Sixty microsecond pulses were transmitted with a peak power of 2.5 megawatts. The pulse repetition frequency was 90 pulses per second. The antenna beam was vertically oriented. At F-region heights the beam is about a kilometer in diameter so that the scattering volume in space was a cylinder of 9 kilometers long and about one kilometer wide. Both the ion and electron components of the backscattered power spectrum were recorded on digital tape.

SECTION III. OBSERVATIONS

A. Data Collection

The network of three phase-path sounders was available for the months of May, June, and July 1967. During this time, observations were made whenever time on the 430 MHz radar could be obtained during daylight hours (0700-1900 local time). Daytime operation was required because the electron component of the back-scattered power spectrum (the "plasma line") is only detectable when it is enhanced by the daytime flux of photoelectrons. In all, 263 hours of observing time were scheduled and of this, all equipment worked satisfactorily during 185 hours.

B. Data Reduction

All usable data have been reduced and examined. The incoherent backscatter observations were reduced at AIO to contour plots of constant plasma frequency versus height and time. The HF observations on both frequencies and from each station were reduced at Raytheon to spectrograms of Doppler shift versus time for various range gate positions. Events of special interest were recycled through the data reduction process one or more times to optimize the presentation.

C. Results

1. Summary

Travelling ionospheric disturbances are found to be a common feature of the daytime ionosphere. Roughly half of the HF Doppler data contain anomalies which can be followed from station to station with little change in form. The statistics of the observations will be discussed in some detail in the final report where correlations with possible geophysical sources will be sought. For the purposes of this report, the data as a whole is summarized simply by tabulating the speed and direction of all prominent events. The velocities have been computed from hand-scaled time delays between stations. The results are shown in Table 1. The computed velocities are quite comparable to those found in earlier studies.[2] It is concluded that the disturbances observed in this study are of the same type as

Table 1. Horizontal Velocities of the Ionospheric Disturbances

Date	Time (U.T.) Hr. Min.	Speed (M/S)	Bearing (Deg. West of North)
5-07-67	13 : 14	66.61	4.36
5-12-67	14 : 50	225.52	55.16
5-14-67	11 : 35	218.32	17.60
5-18-67	21 : 40	148.10	231.21
5-20-67	13 : 30	169.47	83.40
5-21-67	12 : 25	154.30	76.20
5-24-67	21 : 20	218.32	197.60
5-25-67	22 : 45	679.50	55.20
5-27-67	21 : 05	680.00	55.00
5-30-67	22 : 55	428.30	141.16
6-01-67	13 : 48	197.74	60.44
6-03-67	22 : 38	85.73	192.45
6-08-67	13 : 45	374.74	159.00
6-08-67	22 : 49	124.31	191.20
6-14-67	12 : 00	112.70	124.50
6-15-67	12 : 39	172.41	129.50
6-15-67	13 : 35	124.46	41.76
6-18-67	22 : 48	177.50	101.00
6-19-67	22 : 54	179.04	149.18
6-24-67	23 : 00	226.07	177.84
6-27-67	1 : 10	277.58	170.4
6-27-67	22 : 10	122.75	169.10
6-28-67	16 : 55	138.79	350.44
6-28-67	20 : 52	180.50	199.14
6-30-67	13 : 30	107.20	126.58
7-07-67	11 : 57	130.82	48.16
7-08-67	11 : 12	141.43	113.99
7-12-67	13 : 38	159.53	172.17
7-13-67	12 : 32	275.81	15.24
7-15-67	13 : 25	161.41	186.47
7-16-67	11 : 50	132.24	37.24

Table 1 Cont.

Date	Time (U.T.)	Speed (M/S)	Bearing (Deg. West of North)
	Hr. Min.		
7-21-67	22 : 22	186.46	191.20
7-22-67	13 : 02	191.69	34.25
7-29-67	14 : 15	155.55	107.93
7-31-67	19 : 33	201.42	159.00
8-01-67	22 : 10	187.28	174.52

those studied extensively in the past. A test of the acoustic-gravity wave interpretation, based on the data recently collected is therefore believed applicable to earlier observations as well.

2. Examples

Three cases were observed of what may be called "classical" travelling ionospheric disturbances. These are classical in the sense that when HF experimenters wish to give an example of their data, a disturbance of this type is usually shown.[6, 7] These events are characterized by "switch backs" on plots of Doppler shift versus time (or group path versus time if this parameter is analyzed). While these events are more spectacular than most, it is clear that they differ from disturbances which produce single-valued Doppler signatures only in that the horizontal gradients of electron density they cause are slightly greater. This usually means that the wave is high in amplitude and therefore will be easily recognized with incoherent backscatter. Multiple valued disturbances have therefore been given special attention in this report.

The first example is shown in Figure 2. There are two major disturbances here, one at 1410-1425 and one at 1430-1445. The Doppler shift is multiple valued during these periods, indicating that the contours of constant electron density in the ionosphere are distorted enough so that multiple reflections take place. Time shifts of a few minutes are observed between stations. The corresponding incoherent backscatter data is shown in Figure 3. The contours of constant plasma frequency are derived directly from the ion component of backscattered power and normalized to the critical frequency at the layer peak as read from ionograms taken simultaneously. The ionosphere is clearly affected by waves over a considerable height range including the level of HF reflection (about 200 kilometers for 5.228 MHz). The phase fronts of the waves are tilted forward as expected from earlier incoherent backscatter results.[3]

The second example is shown in Figure 4. The time scale, Doppler shift structure, and time delays between stations are similar to the event just discussed. Unfortunately, the 430 MHz radar at AIO was not operable during this event and the incoherent backscatter data is not available.

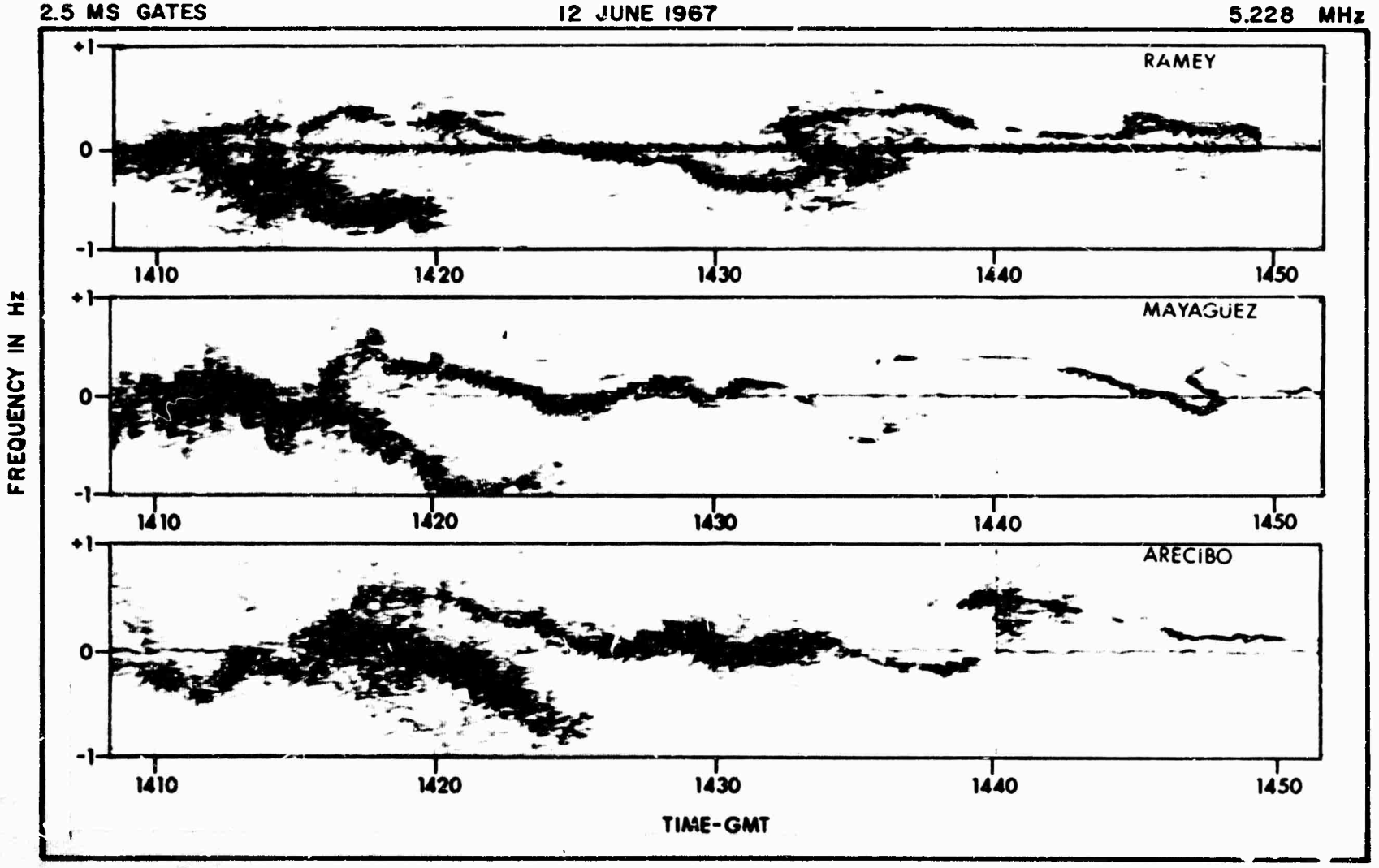

Figure 2. Doppler Shift Records at the Three Sites on June 12, 1967 Using an Operating Frequency of 5.228 MHz

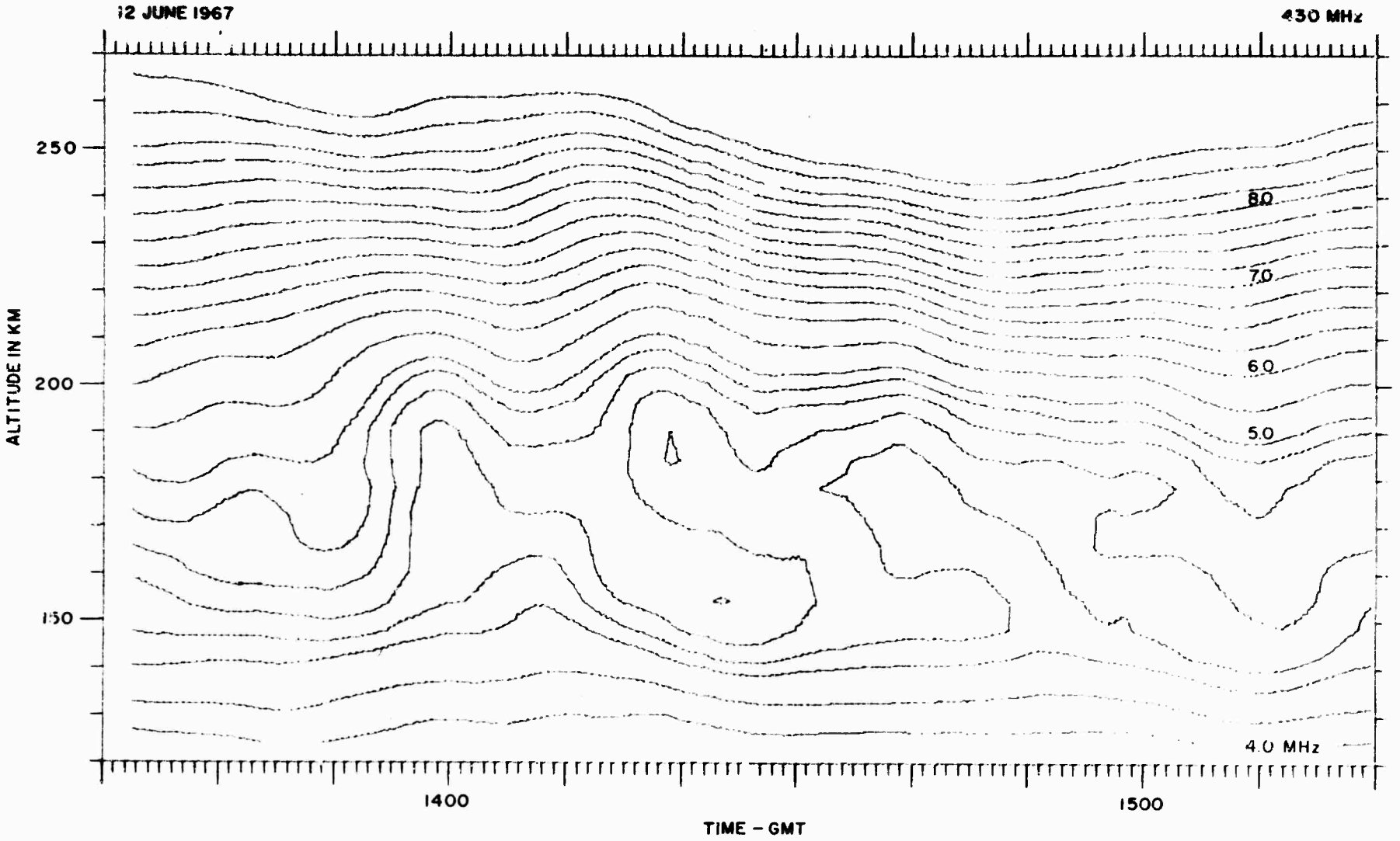

Figure 3. Contours of Constant Plasma Frequencies from Incoherent Backscatter Measurements at 430 MHz on June 12, 1967

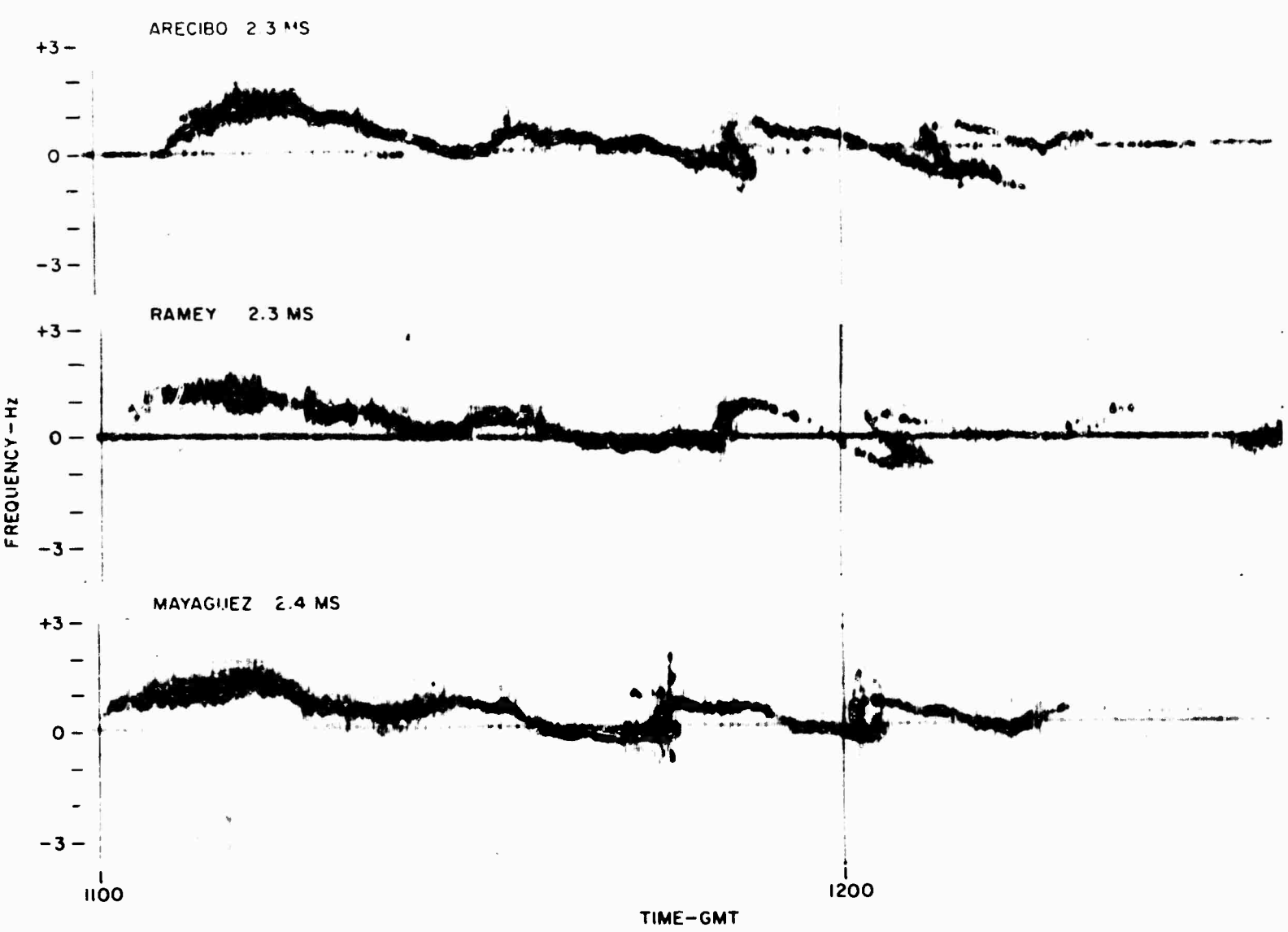

Figure 4. Doppler Shift Recordings on June 14, 1967 at an Operating Frequency of 6.843 MHz

The third example is shown in Figure 5. The classical events occur about 1110 and 1125. The data from 1130 to 1400 is shown because it corresponds to a major wave event on the incoherent backscatter data. The backscatter data is shown in Figure 6. The diamonds and connecting lines between 250 and 300 kilometers indicate the height of the F-region peak. The "islands" at the peak which form at about 1140, 1225, and 1305 represent condensations caused by a train of travelling waves. The sloping phase fronts of the wave crests are evident. During much of this disturbance, the HF ray paths were severely distorted and reliable measurements of wave velocity can not be made using hand scaled delay times between stations. It is expected, however, that the cross-correlation analysis which would be extended to this data during the next phase of the study will provide meaningful measurements of the velocity throughout this event.

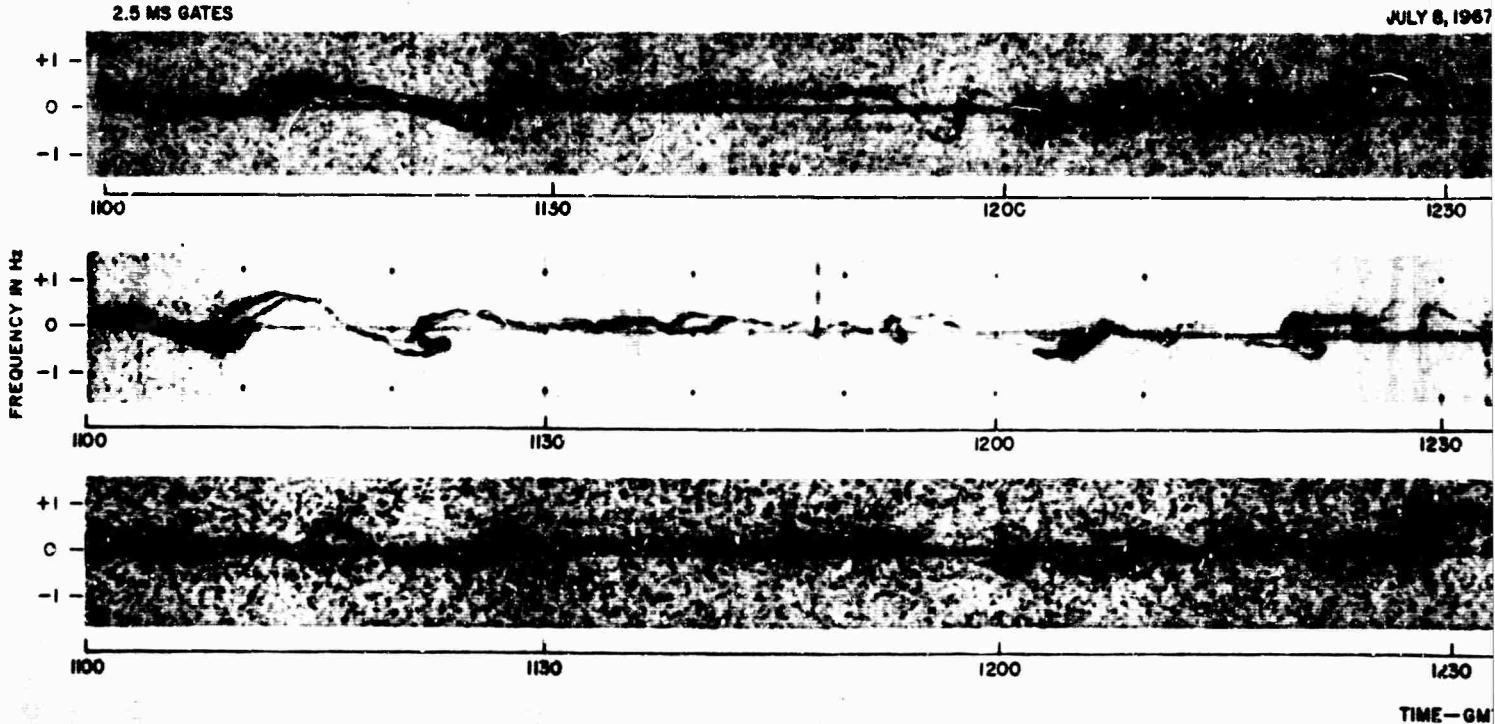
2.5 MS GATES
JULY 8, 1967
+1
0
-1
1100
1130
1200
1230
FREQUENCY IN Hz
+1
0
-1
1100
1130
1200
1230
+1
0
-1
1100
1130
1200
1230
TIME—GM

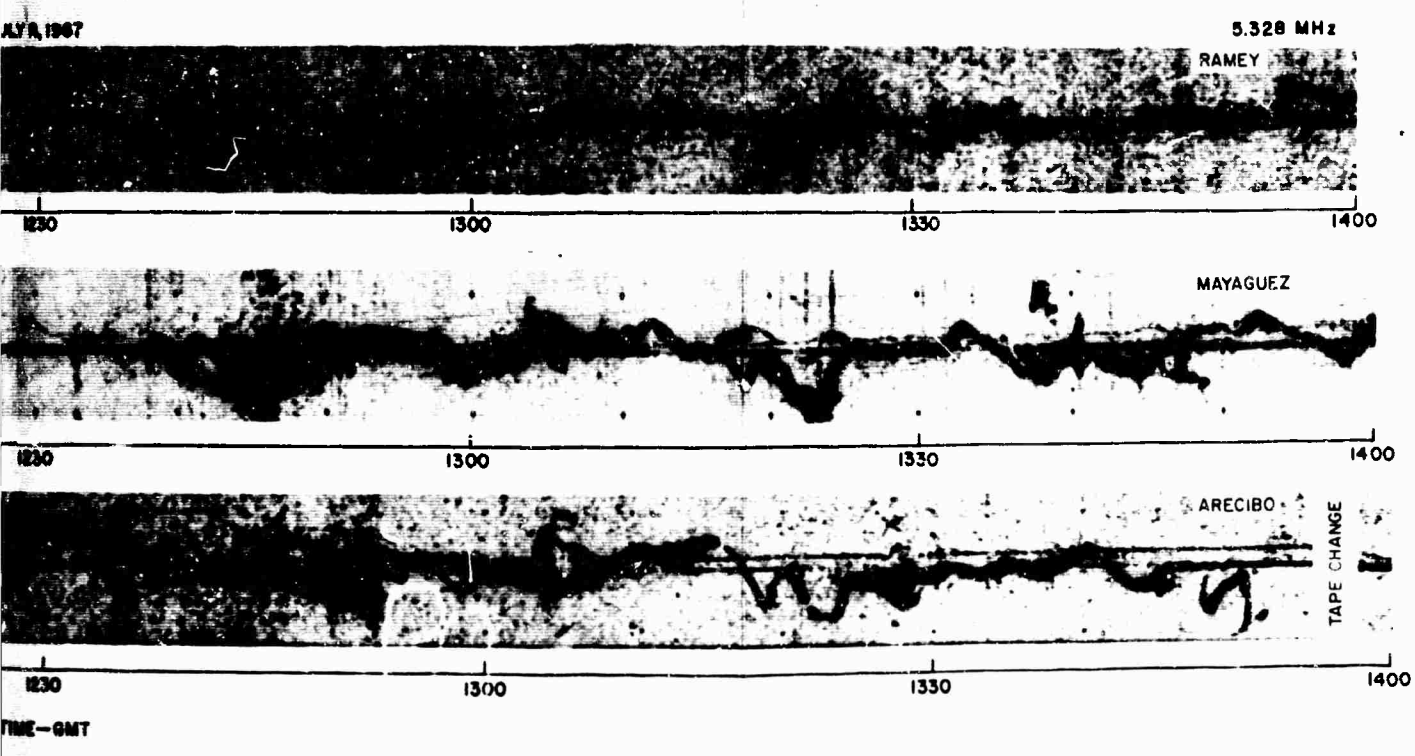

Figure 5. Doppler Shift Recordings on July 8, 1967 at an Operating Frequency of 5.328 MHz

BLANK PAGE

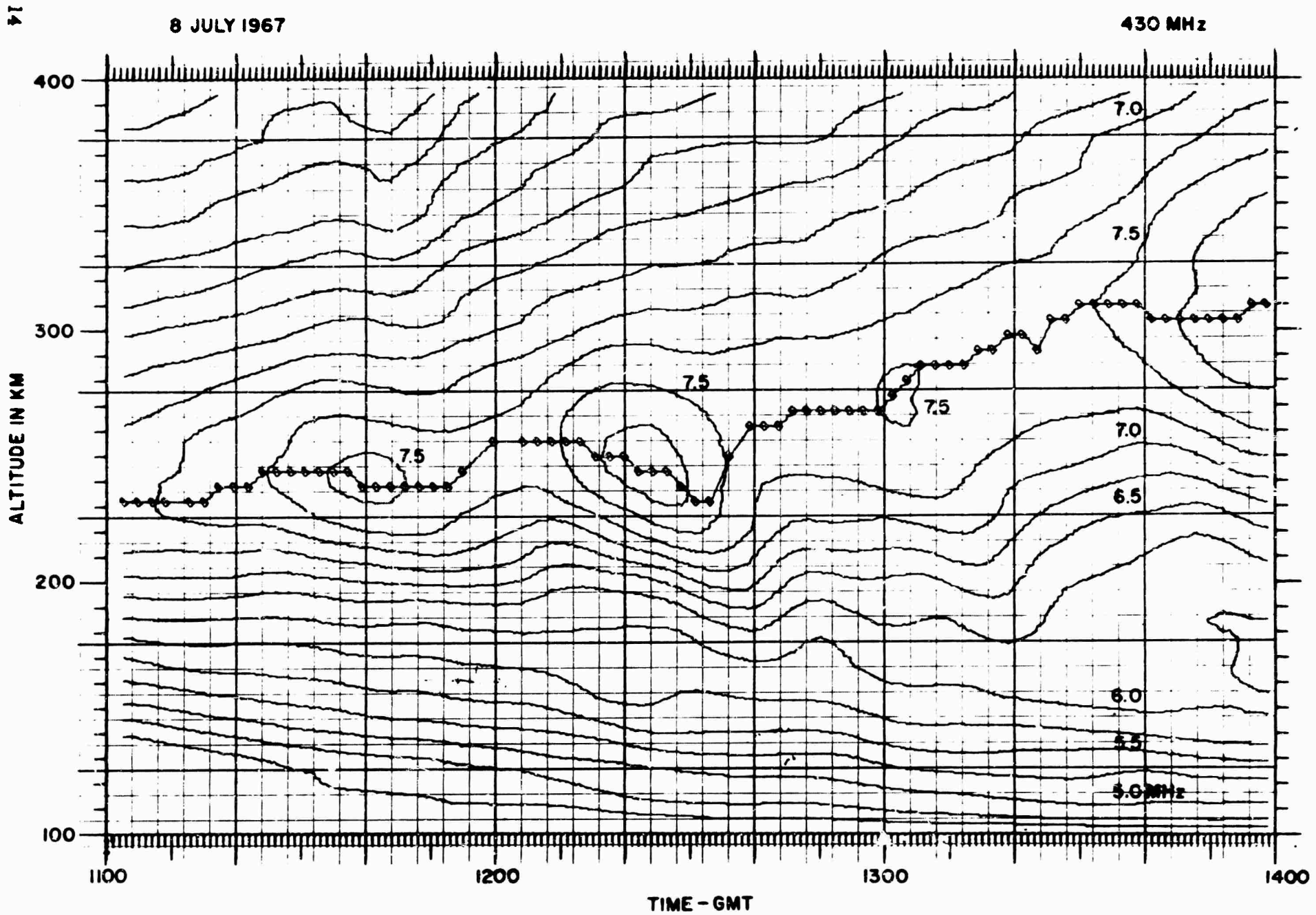

Figure 6. Contours of Constant Plasma Frequencies from the Backscatter Measurements on July 8, 1967

SECTION IV. ANALYSIS

The event of 12 June 1967 is representative of the 3 classical travelling ionospheric disturbances observed and will be used for a comparison with acoustic-gravity wave theory. The analysis is based upon three distinct techniques: Cross correlation for an objective measurement of the wave velocity, ray tracing for demonstrating the self-consistency of the HF and the incoherent backscatter data, and the coupling of acoustic gravity waves to the ionospheric plasma. The techniques themselves are discussed in the appendix and referred to in the analysis when used.

The HF and incoherent backscatter data for June 12 have been shown in Figures 2 and 3 respectively. The first step in the analysis is to derive the horizontal velocity of the wave by cross correlation of the HF signatures. The HF signatures have been digitized by hand to provide a one-bit representation for the computer. Figure 7 shows the digitized signals at the three stations. The cross-correlation program is described in Appendix A. Figure 8 shows the result for the 20 minute window containing the first and largest signature. The derived speed is 112 m/s. The direction of travel is from 75° west of north.

The next step in the analysis is to use the derived speed to convert the time axis of the incoherent backscatter data (Figure 3) to horizontal distance. This defines a two-dimensional distorted ionosphere which moves overhead at a known speed. The assumption of two-dimensionality is equivalent to assuming that the disturbance is a plane wave and past studies have shown this to be at least approximately true.[2]

At this point a check on the self-consistency of the experimental data has been made by doing ray tracing through the distorted ionosphere to synthesize the HF signature observed at Arecibo. The ray tracing program is described in Appendix B. The result is shown in Figure 9. The match is felt to be surprisingly good considering the many idealizations made to this point and it is concluded that the experimental data is self-consistent.

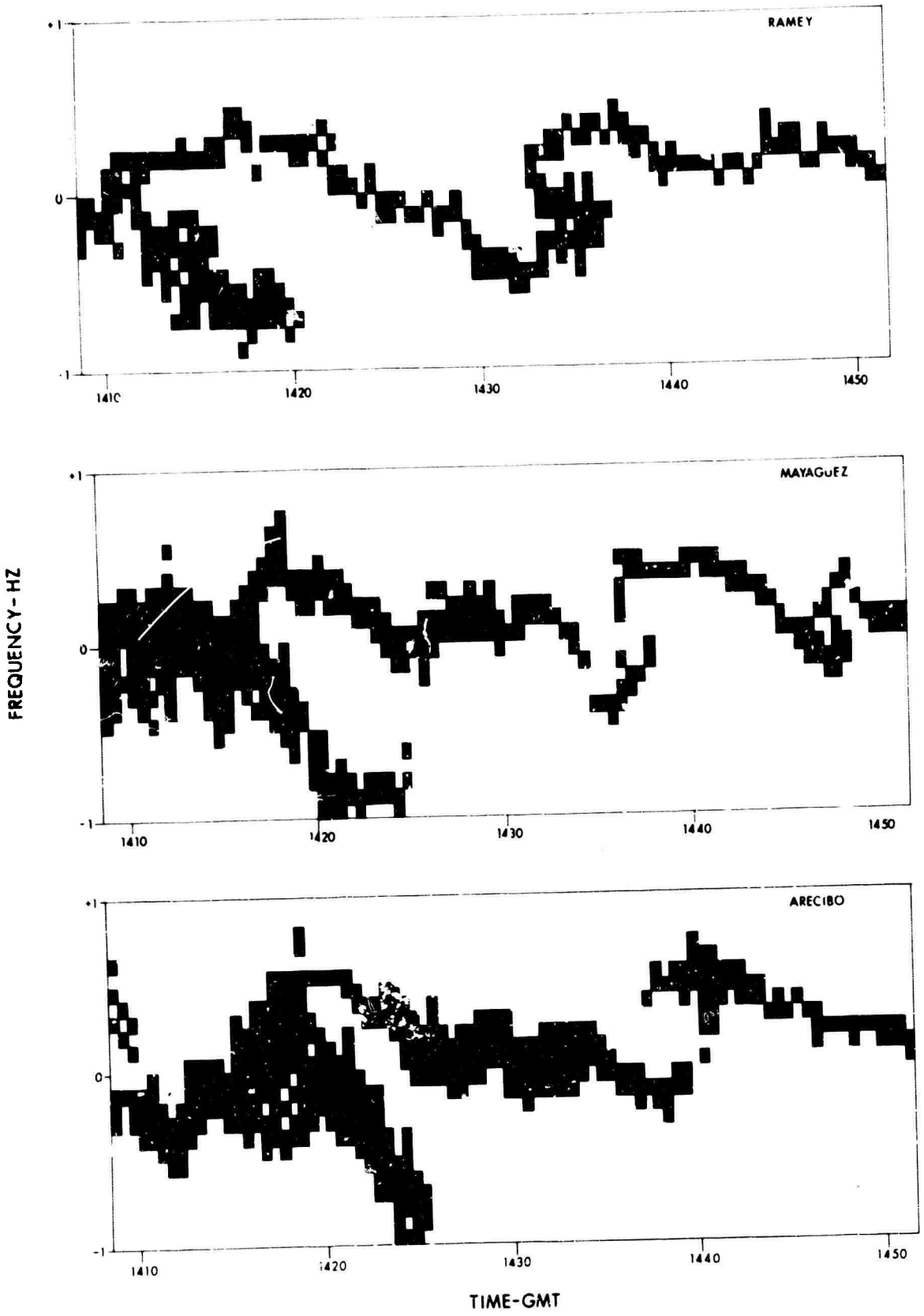

Figure 7. One-bit Digitized Version of the Doppler Shift Signatures of June 12, 1967

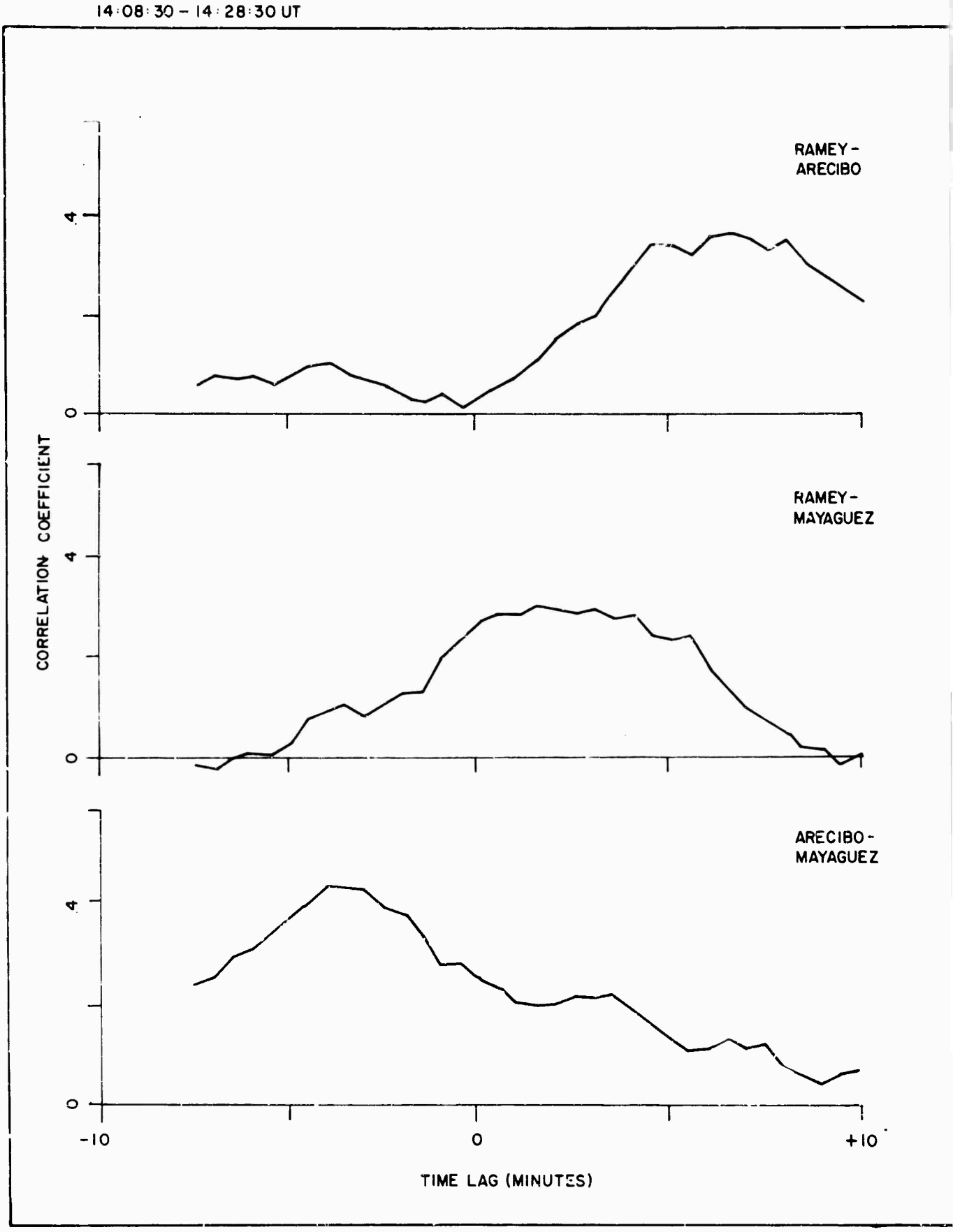

Figure 8. Cross Correlograms for the 3 Pairs of Stations for a Selected 20 Minute Window Centered on the Main Signature of the Digitized Doppler Record

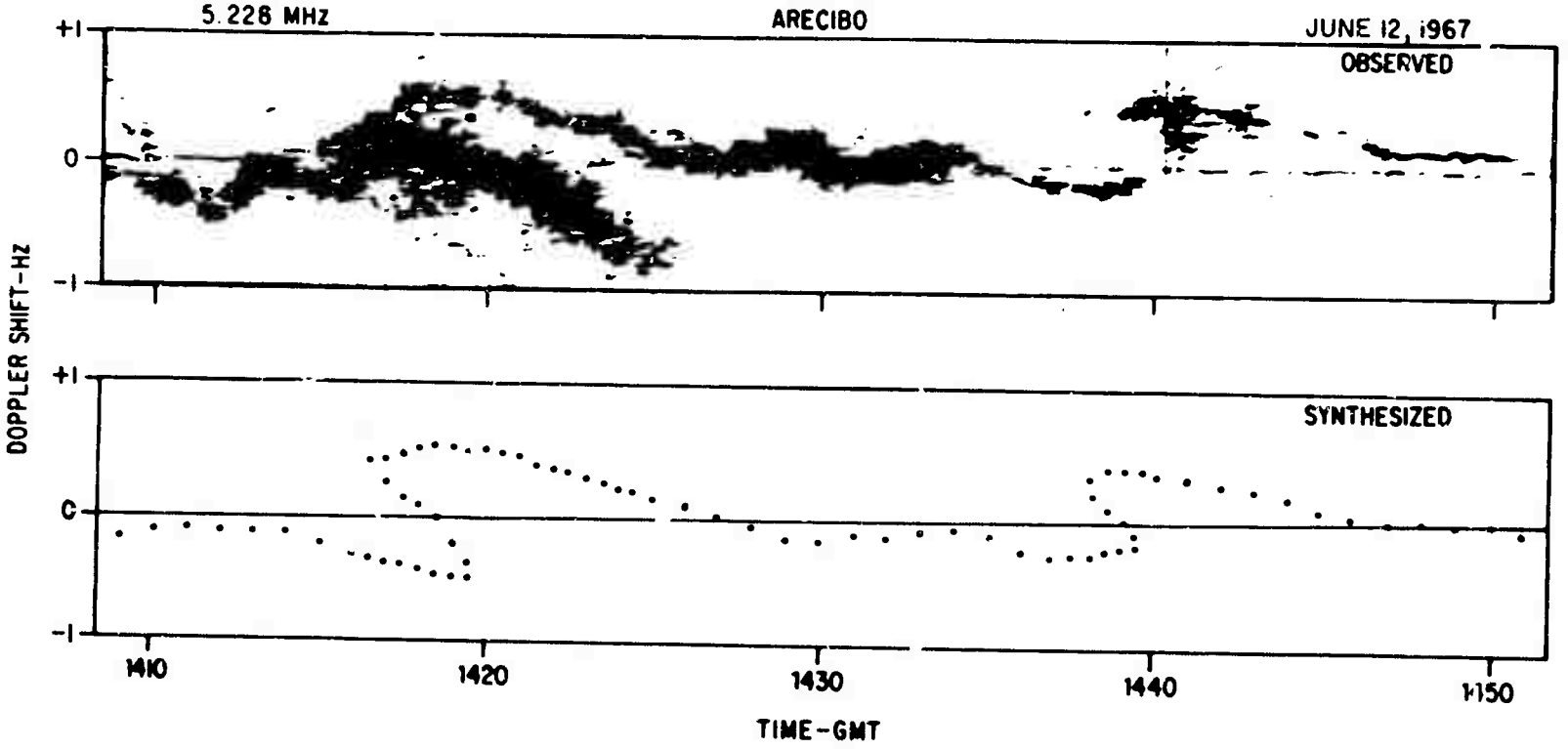

Figure 9. Observed and Synthesized HF Doppler Signatures of June 12, 1967

Figure 10 compares the reflection level for the HF radar (ordinary ray) as derived from incoherent backscatter with the HF signatures observed at Arecibo. Clearly, the signature is associated with the concave ripples in the contours. The wave period is about 20 minutes and the wave length about 146 kilometers. Figure 11 shows the level of reflection with the appropriate distance scale added. Also shown is a line of constant phase predicted by acoustic-gravity wave theory. The equation shown on this figure is the dispersion relation for such waves where K_z is the (complex) vertical wave number, ω_B is the angular brunt frequency of the neutral atmosphere, ω is the angular wave frequency, K_x is the (real) horizontal wave number, H is the neutral scale height, and is the kinematic viscosity of the neutral gas. This equation neglects phase shifts due to production and recombination but is correct to first order. The derivation including these processes is given in Appendix C. Theory predicts that at all altitudes the trough of the wave should fall along the dashed line.

Contours of constant plasma frequency over the entire height range are shown in Figure 12. Agreement between the position of the wave trough and the dashed line is seen to be very good. Qualitatively, the wave amplitude should grow exponentially with altitude until viscous damping becomes important. As damping sets in, the lines of constant phase should swing towards the vertical and the wave amplitude should drop. The swing to the vertical is observed to occur in the range 200-250 kilometers altitude and the amplitude of the disturbance is also observed to drop in the same interval. The agreement between acoustic-gravity wave theory and the observed travelling disturbance structure is taken as strong evidence for the correctness of this interpretation.

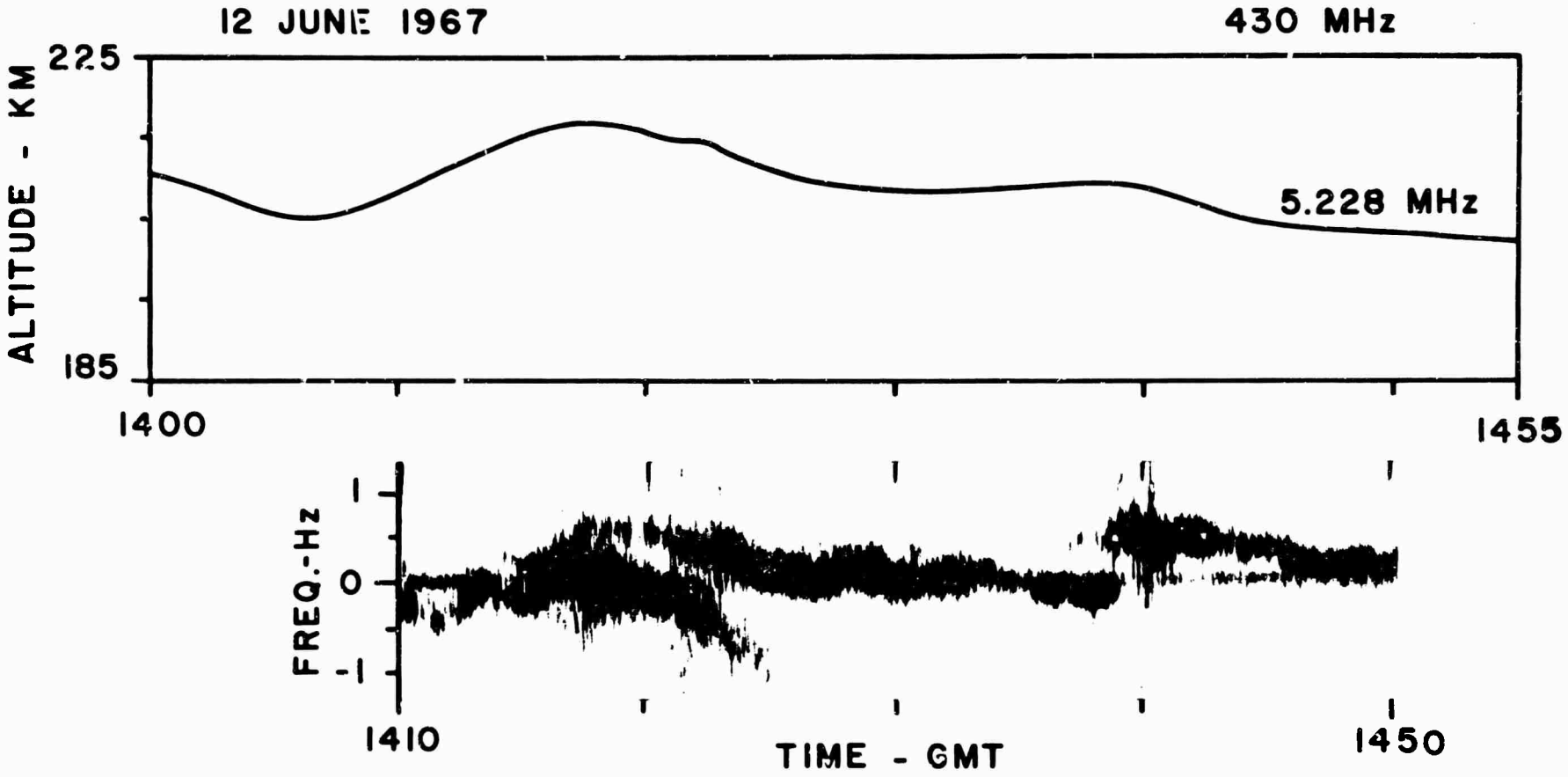

Figure 10. Comparison of Variations in 5.228 MHz Reflection Level with the HF Signature at the Same Frequency at Arecibo

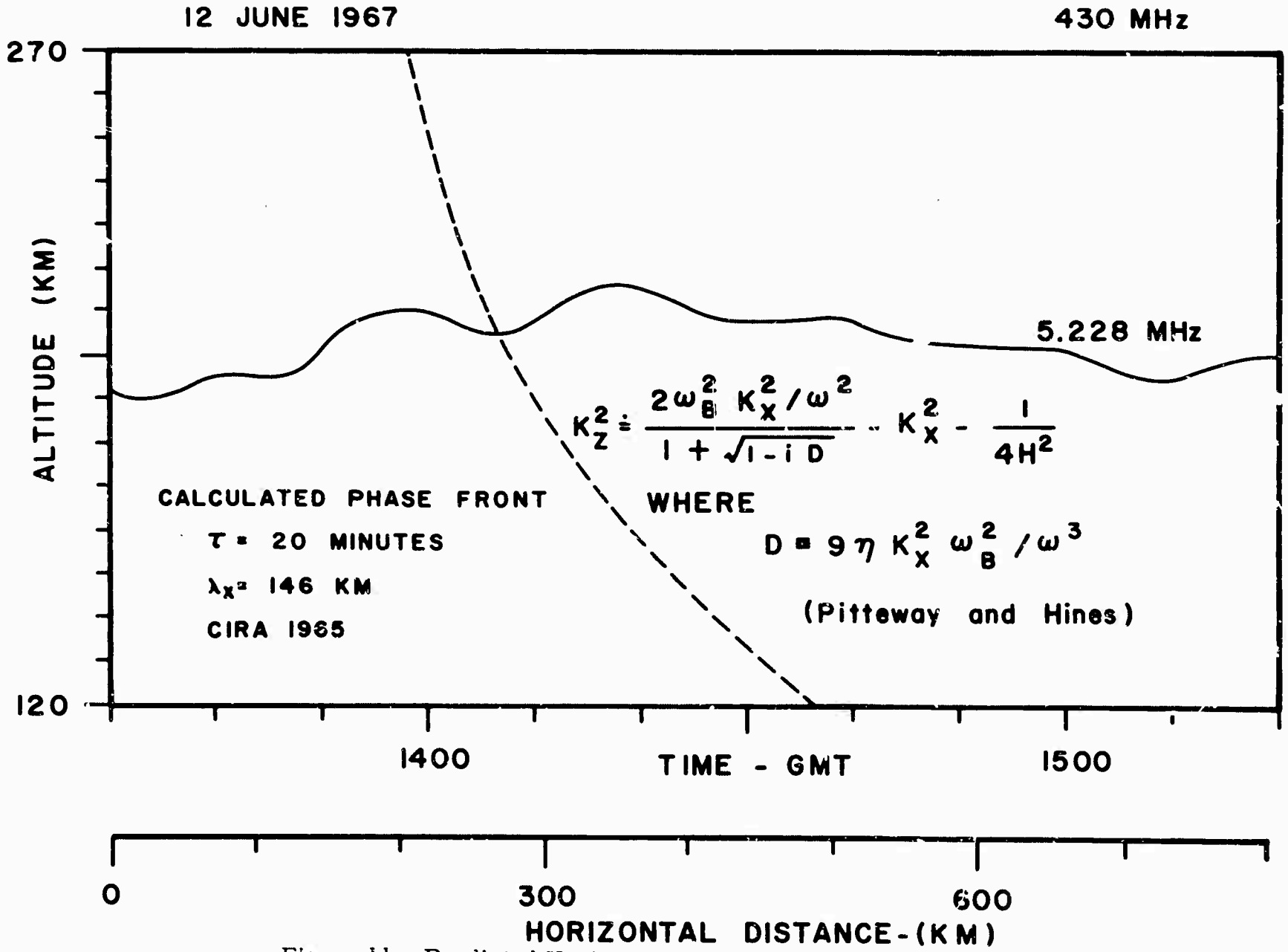

Figure 11. Predicted Variation of the Phase of an Acoustic Gravity Wave with Altitude

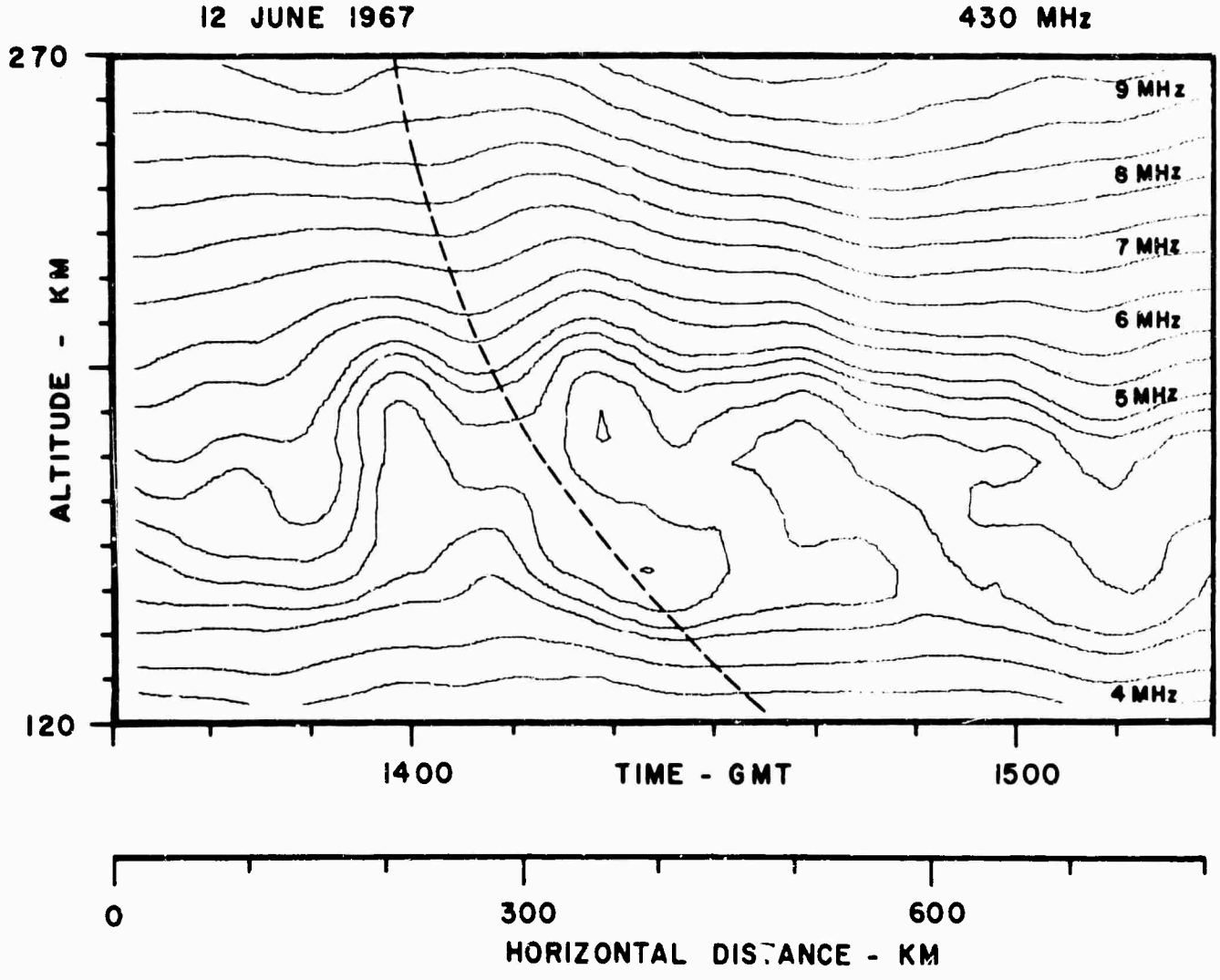

Figure 12. Comparison of Predicted and Observed Phase Variation with Altitude

SECTION V. CONCLUSIONS

It is concluded that large scale travelling ionospheric disturbances are acoustic-gravity waves. No significant discrepancies between theory and observation have been found. In the final phase of this study, some aspects of the analysis will be refined, such as including loss and production terms when coupling the neutral wave to the ionospheric plasma. It is clear, however, that while such refinements may point up areas which need more theoretical work, the acoustic-gravity wave interpretation itself is on firm ground.

Future plans for the remaining portion of this study include three tasks. First, the comparison between theory and observation will be refined as described above. Second, the assumption (usually made in HF studies) that all important Doppler shift anomalies are introduced at or near the reflection height will be examined. Third, a search for the wave sources will be made by looking for correlations between the observed events and other geophysical disturbances occurring at the proper time and place.

SECTION VI. APPENDIXES

A. Cross Correlation

Horizontal velocity of a travelling ionospheric disturbance is determined by measuring time delays in the occurrence of similar complex signatures on the Doppler shift records obtained at the three spaced sites as stated in Section III (c). The determination of the time lags by lining up the similar signatures on the 3 Doppler shift records involves a certain degree of subjective error especially when the signatures extend considerably in time and are not of identical configuration on the 3 tracks. A statistical approach involving the calculation of cross correlation functions between each pair of the Doppler records is desirable in situations like this to extract the best estimates of the time delays and thereby the required velocity information. The cross correlation analysis is, in fact, widely used for studying the structure and movement of the small scale irregularities from the observed 3 station amplitude fading patterns of a reflected radio signal[8, 9]. The Doppler data collected on June 12, 1967, which exhibited a distinct loop type complexity at the 3 stations, is subjected to the correlation analysis as described below. Unlike the amplitude patterns, the Doppler shift of a received signal can have multiple values at any given instant of time and this in priciple leads to a correlation function in the two dimensions of time and frequency. In the present analysis, however, the correlation functions are calculated in the single dimension of time only for the case of zero relative shift in the frequency (i. e. $\Delta f = 0$). In order to perform the correlation, the analog Doppler record has to be digitized or sampled in time and frequency. For this purpose the time and the frequency axes are scaled at intervals of 1/24 Hz and 30 secs, respectively. The digitization of the signal is accomplished by assigning the Doppler shifts of the signal either 1 or 0, depending on whether the signal is present or not in the given cell of frequency-time grid. The analog and digitized versions of the Doppler shift records at the 3 stations have been shown in Figures 2 and 7 respectively (Sections III (c) and IV). The course digitization might have some smearing effect on the correlation functions but it is not expected to cause

any significant difference in the measurement of the time delays. The one-bit digitized Doppler values are denoted as $P_1(t, f)$, $P_2(t, f)$ and $P_3(t, f)$ for the 3 stations -- Ramey, Arecibo and Mayaguez. The cross correlation function for any pair of signals $P_A(t, f)$ and $P_B(t, f)$ corresponding to a time lag of Δt is expressed as:

$$\rho_{A,B}(\Delta t) = \frac{\left\langle \left[P_A(t,f) - \overline{P_A(t,f)} \right] \left[P_B(t+\Delta t, f) - \overline{P_B(t,f)} \right] \right\rangle}{\left\{ \left\langle \left[P_A(t,f) - \overline{P_A(t,f)} \right]^2 \right\rangle \right\}^{1/2} \left\{ \left\langle \left[P_B(t,f) - \overline{P_B(t,f)} \right]^2 \right\rangle \right\}^{1/2}}$$

$$\overline{P_A(t,f)} = \frac{1}{f_0} \frac{1}{(t_2 - t_1)} \sum_{f=1}^{f=f_0} \sum_{t=t_1}^{t=t_2} P_A(t,f)$$

$$\overline{P_B(t,f)} = \frac{1}{f_0} \frac{1}{(t_2 - t_1)} \sum_{f=1}^{f=f_0} \sum_{t=t_1+\Delta t}^{t=t_2+\Delta t} P_B(t,f)$$

where f_0 is the total number of frequency scalings and $(t_2 - t_1)$ is the length of selected window for correlation. In the present analysis $f_0 = 24$ and $(t_2 - t_1) =$ 20 minutes. The cross correlation functions $\rho_{12}(\Delta t)$, $\rho_{13}(\Delta t)$ and $\rho_{23}(\Delta t)$ between the pairs of stations Ramey-Arecibo, Ramey-Mayaguez and Arecibo-Mayaguez are computed for Δt varying from -10 to +10 minutes in steps of one minute. In Figure 13 are shown the plots of the correlation functions for six different correlation windows each removed from the other by 5 minutes over the total test interval 14:08:30 - 14:53:30 U. T. The plots reveal that over the interval 1408-1433 corresponding to the first two correlation windows during which the major complexity of the Doppler shift occurred, the correlations for all the 3 pairs of stations are found to be high. During the later periods, however, the correlation is found to remain significant only between Arecibo-Mayaguez while for the other two pairs the correlation has degraded rapidly with time. Low

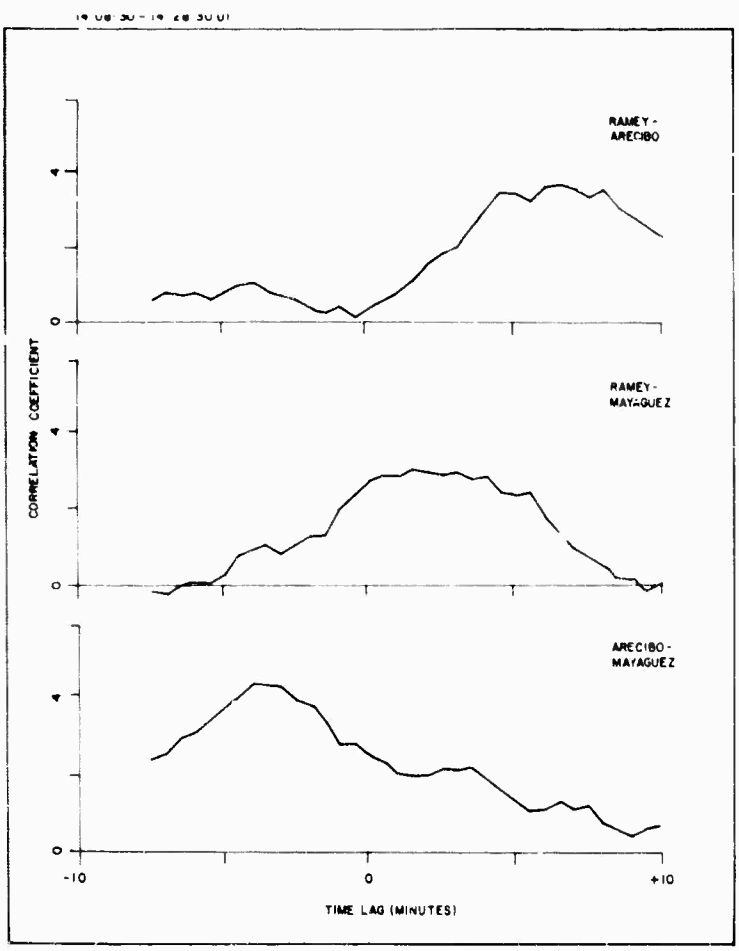

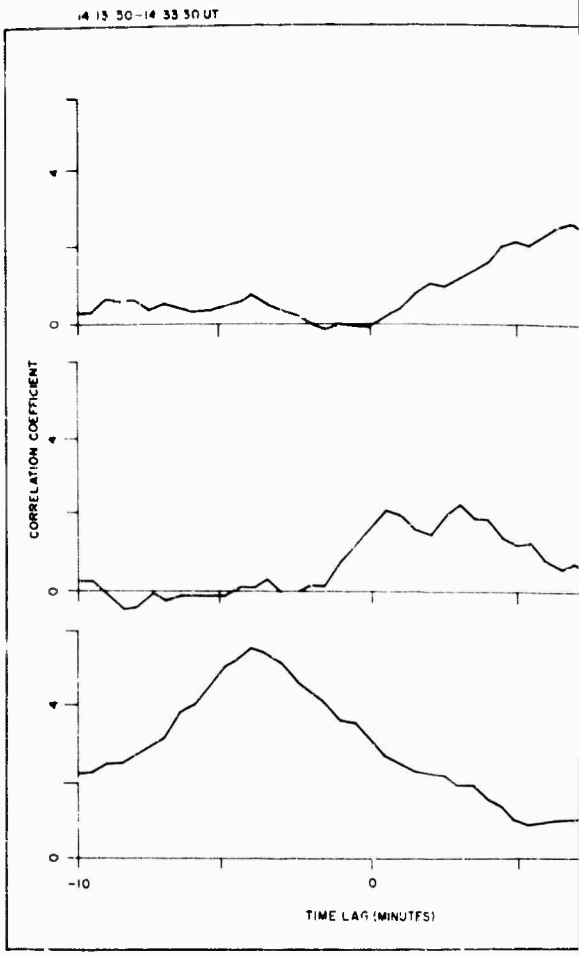

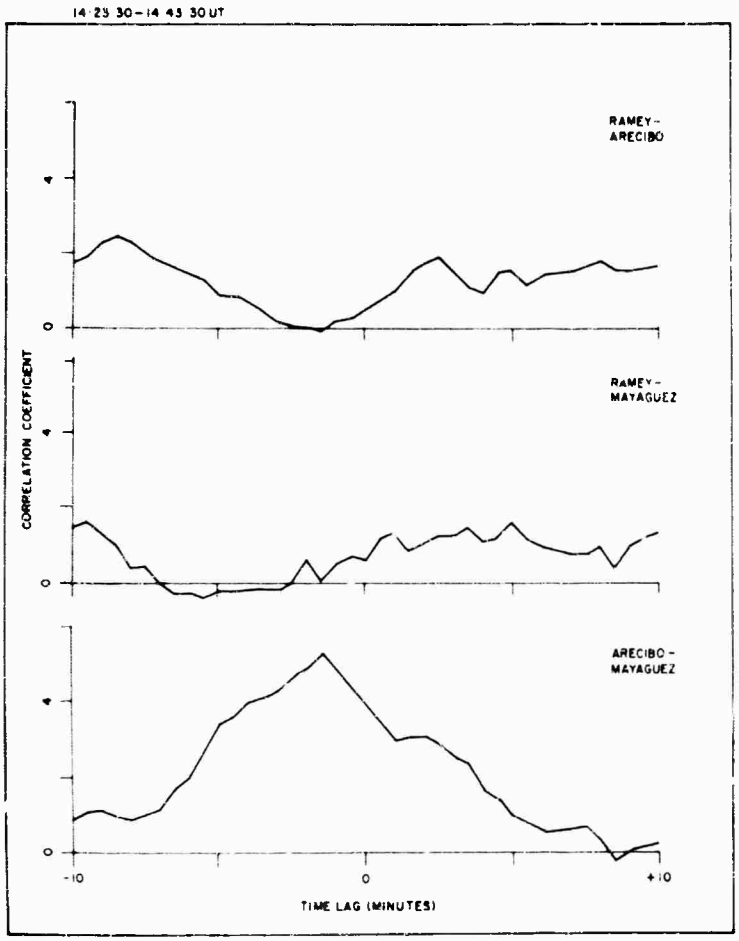

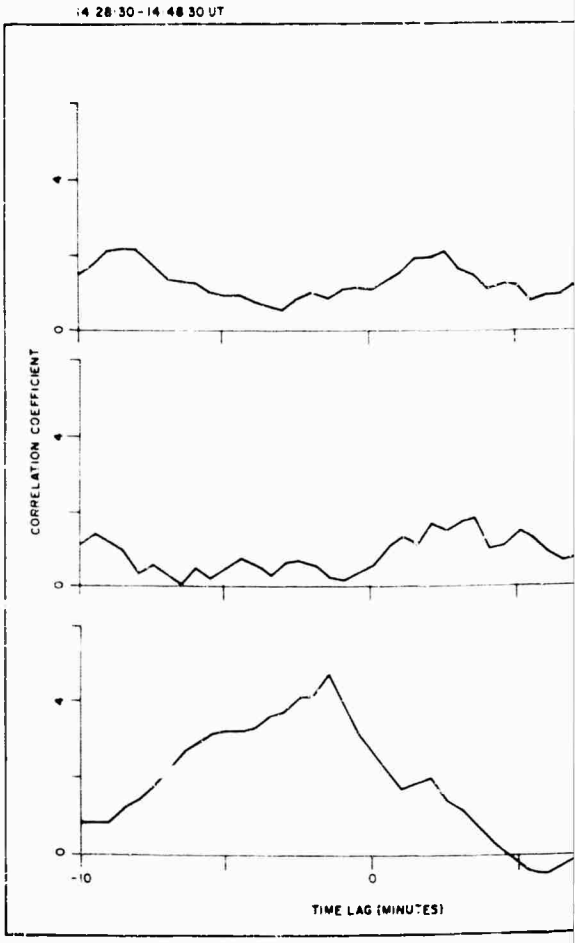

Figure 13. Cross Correlograms for Six Successive Positions of a 20 Minute Running Window in the Test Interval 14:08:30 - 14:53:30 U. T. on June 12, 1967

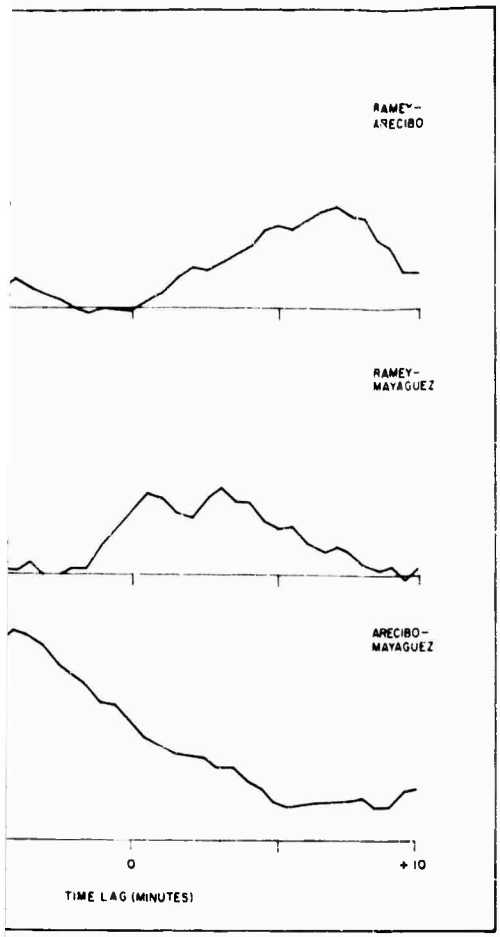

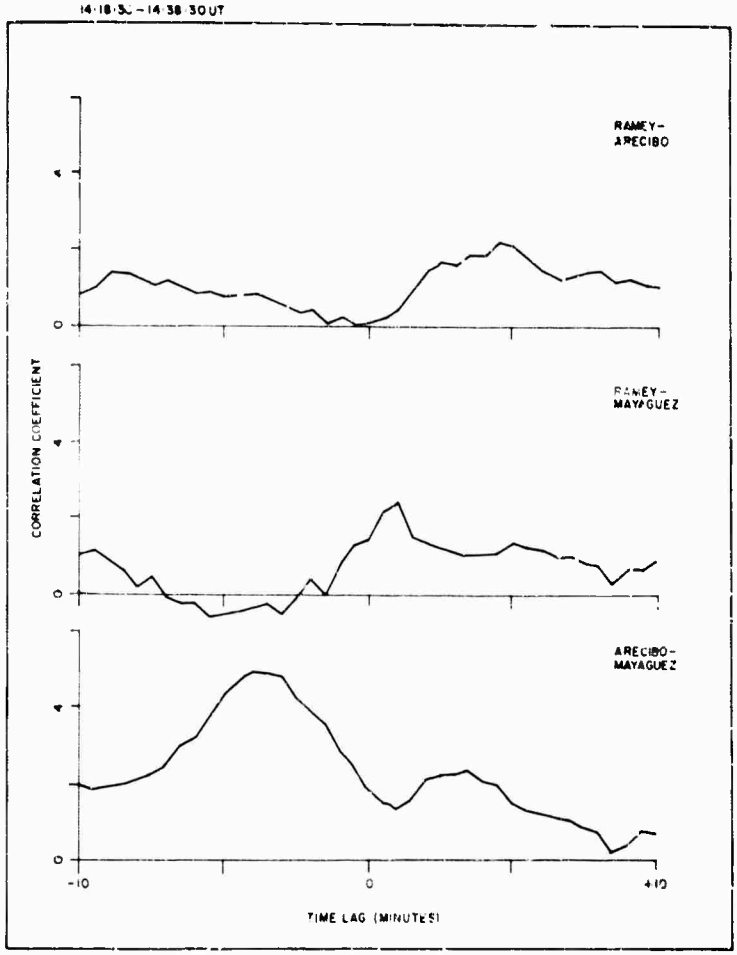

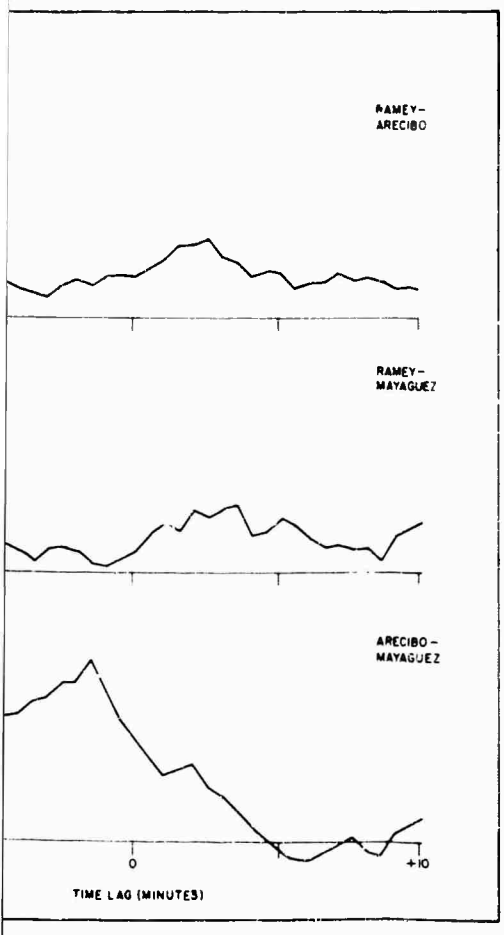

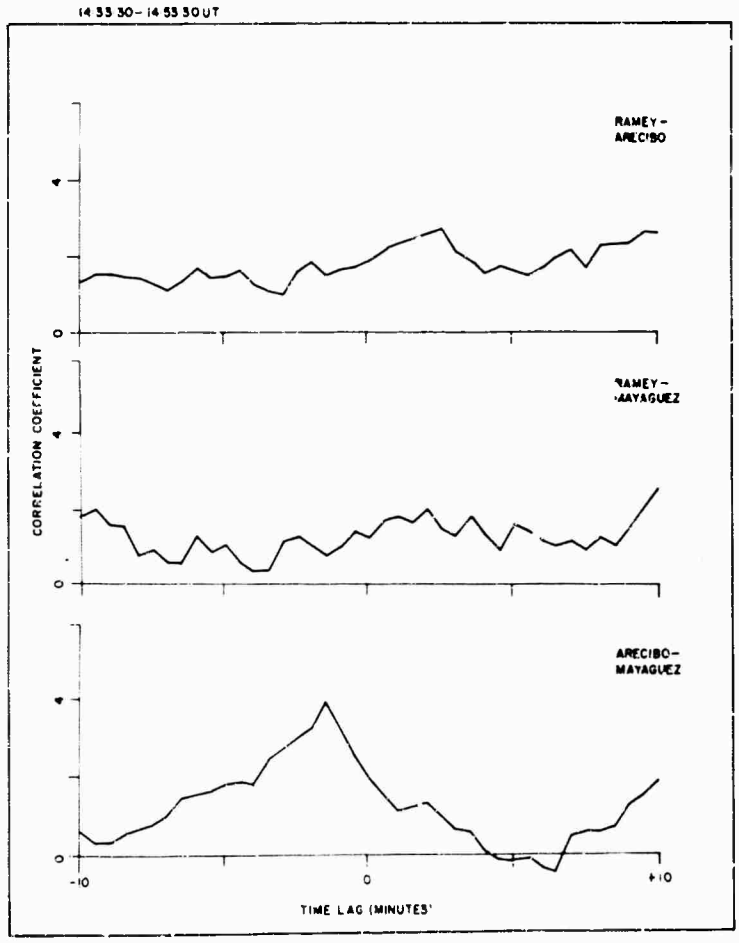

ns of a
14:08:30 -

BLANK PAGE

correlation between any pair of the stations would normally mean that the disturbance front is small in dimension compared to the receiver separation or that the shape of the disturbance is changing rapidly compared to the travel time of the disturbance from one receiver to the other. The information about the speed and direction of the disturbance that imposed the major complex signature at 1420 U.T. is derived from the first correlation window which furnishes the correlation coefficients of highest significance. The velocity is calculated from the following equations using the station geometry, and the time delays derived from the correlation analysis.

$$\tan \theta = \left(\frac{x_{13}}{x_{12}} \right) \left(\frac{\tau_{12}}{\tau_{13}} \right) \left(\frac{1}{\sin \alpha} \right) - \cot \alpha$$

$$S = \left(\frac{x_{13}}{\tau_{13}} \right) \cos \theta = \left(\frac{x_{12}}{\tau_{12}} \right) \cos (\alpha - \theta)$$

where:

x_{12} and x_{13} are the distances between stations 1-2 and 1-3 respectively.

τ_{12} and τ_{13} are corresponding time delays.

α is the angle between the paths joining 1-2 and 1-3.

θ is the direction of propagation of the disturbance measured counter-clockwise from the line joining the stations 1 and 3, and

S is the speed of propagation of the disturbance. The velocity and the parameters pertinent to the calculation are listed below.

x_{12} = 44 km $\quad \tau_{12}$ = 6.25 Min. $\quad$ S = 112 m/s

x_{13} = 32 km $\quad \tau_{13}$ = 1.50 Min. $\quad$ Bearing = 75° west of north

B. Ray Tracing

1. Specification of the Electron Density Distribution in the Ionosphere

The observed ionosphere is read into the computer as a two dimensional (height-time) array of plasma frequencies. The interval between adjacent points is 6 kilometers in height and 33 seconds in time. Once in the computer, the time axis of the array is converted to horizontal distance using the wave speed derived from spaced sounder measurements, the plasma frequencies are converted to electron densities and the array is then in the standard form for ray tracing.

2. Basic Assumptions

2.1 Electron Density Between Grid Points of Input Ionosphere

The electron density between grid points is found by linear interpolation in both space dimensions. Figure 14 gives a physical picture of the interpolation for a typical cell. The X-axis represents horizontal distance, the Z-axis represents altitude, and the N-axis represents electron density. Linear interpolation amounts to passing a plane through the three grid points in the X-Z-N space.

In the X-Z plane the contours of constant electron density are straight lines for a particular cell. Figure 15 shows the contours within two adjacent cells having grid point densities of 8, 9, 12 and 13 (arbitrary units). The electron density is continuous across cell boundaries. The magnitude and direction of the electron density gradient is constant within each cell but may change discontinuously across the boundary.

2.2 Earth's Curvature and Magnetic Field

The earth's curvature and magnetic field are ignored. The neglect of curvature is of no practical consequence for the nearly vertical ray paths of interest. The neglect of the magnetic field is a more restrictive assumption but is felt to be justified by the fact the time displacement between disturbance signatures observed on ordinary and extraordinary rays is always small compared to the wave period and is often undetectable. The lateral deviation of the rays by the magnetic field is therefore of secondary importance. Rays traced using the true operating frequency are identified as ordinary rays for the purpose of comparing the results with observation. Extraordinary rays are traced using the quasi-longitudinal approximation in which the operating frequency is reduced by half the gyro-frequency.

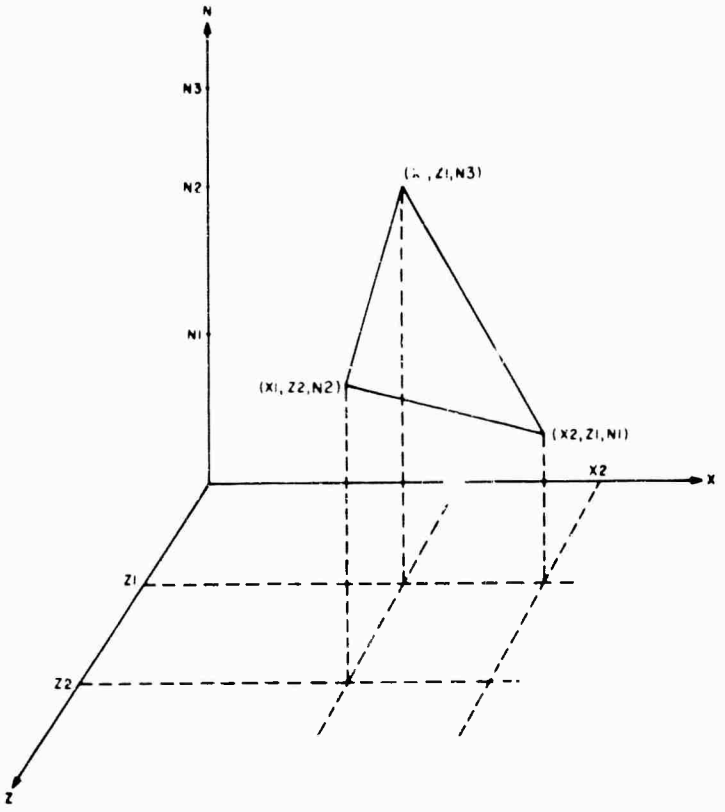

Figure 14. Geometrical Interpretation of the Interpolation Method

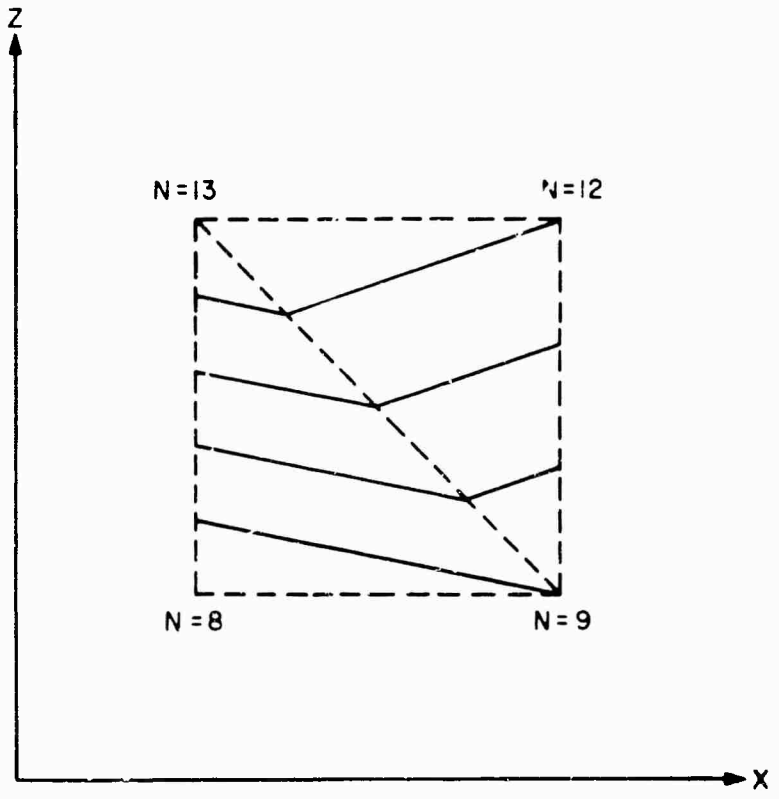

Figure 15. A Representation for Typical Electron Density Cells

3. Ray Tracing Method

3.1 Coordinate Transformation

Under the above assumptions rays follow parabolic paths within each cell.[10] The parabola differs from cell to cell in accordance with the magnitude and direction of the electron density gradient, the operating frequency, and the initial orientation of the ray. The equations become particularly simple when the gradient is vertical, the zero level of electron density is at the ground, and the ray is launched from the origin of the coordinate system. To take advantage of this, the ray is traced through each cell by first transforming the cell from its original X-Z coordinate system to the U-V system in which the simple equations are valid. The transformation consists of a rotation to make the gradient vertical, a vertical translation to make the zero level of electron density lie along the horizontal axis, and a horizontal translation to make the ray pass through the origin. Figure 16 illustrates the translation for a typical cell.

3.2 Ray Tracing Equations in the Transformed System

Let α be the space rate of change of electron density, normalized to the critical electron density for the operating frequency used:

$$\alpha = \sqrt{\left(\frac{\partial N}{\partial X}\right)^2 + \left(\frac{\partial N}{\partial Z}\right)^2} \Big/ N_{crit}$$

In MKS units, $N_{crit} = 1.24 \times 10^{10} (f_{op})^2$ where f_{op} is the operating frequency. Similarly, let β be the time rate of change of electron density normalized to N_{crit}:

$$\beta = (\partial N/\partial t)/N_{crit}$$

Then the ray path is given by

$$U = \frac{\sin 2\theta_0}{\alpha} \pm \frac{2 \sin \theta_0}{\alpha} \{\cos^2 \theta_0 - \alpha V\}^{1/2} .$$

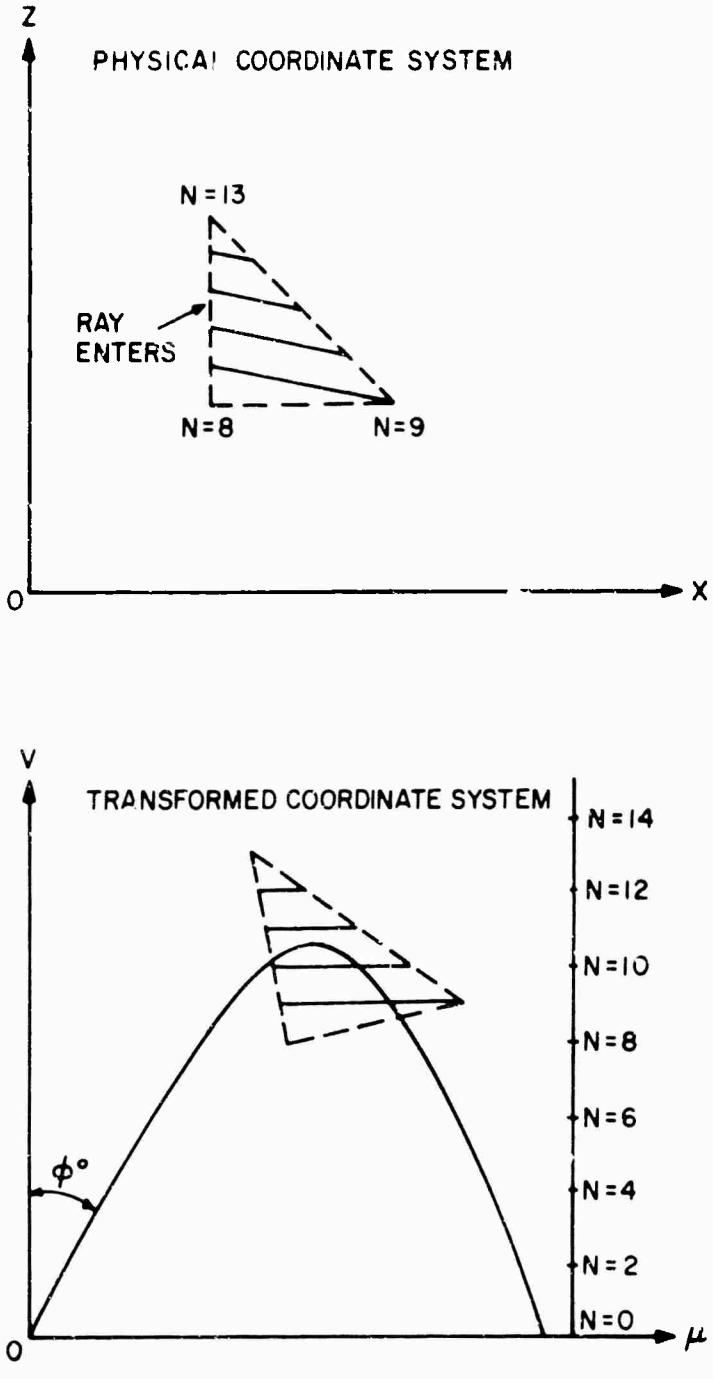

Figure 16. Illustration for Coordinate System Transformation

The phase path length from the origin to any point along the ray is

$$P = \frac{2}{3\alpha} \left[(1+2 \sin^2\theta_0) \cos \theta_0 \pm (1+2 \sin^2\theta_0 - \alpha V) (\cos^2\theta_0 - \alpha_V)^{1/2} \right]$$

The instantaneous Doppler shift imposed along the ray path from origin to observation point is

$$D = -(\beta/\alpha\lambda) \left[\cos \theta_0 \pm (\cos^2 \theta_0 - \alpha V)^{1/2} \right]$$

where λ is the operating wavelength in free space. In all three equations the (+) sign is taken when the observation point lies beyond reflection and the (-) sign when it lies before.

3.3 Procedure

The ray is traced cell by cell. The first step, from ground to ionosphere is a straight line. The impact point on the bottom of the ionosphere determines the first cell entered by the ray. The cell is transformed to the U-V system and the ray path computed. This determines the point at which the ray exits from the cell and its orientation at that point. The phase path length and the Doppler shift are computed from the origin for both the entry and exit points and the results subtracted to give the contribution of the path segment within the cell. The exit point and ray orientation as the ray leaves the cell constitute the entry point and ray orientation for the next cell and the process is repeated until the ray returns to earth. The phase path length and Doppler shift contributions from each cell are added as the ray proceeds. When the ray impacts at the ground the range from the transmitter is noted and the take-off angle of the next ray modified accordingly. After several trials the take-off angle required for the ray to return to the transmitter is found. The ionosphere is then moved horizontally with respect to the transmitter and the process continued until a Doppler shift versus time record has been synthesized for the period of interest.

4. Cost

The calculations involved in tracing a single ray require about one second of computer time (IBM 7044). The cost per ray is about 10 cents.

C. Wave Interaction With Plasma

An atmospheric wave propagating in the ionosphere interacts with the ionospheric plasma and causes perturbations in the electron and ion densities. In this section is developed a simple model for the electron density perturbation in response to an acoustic gravity wave propagating in a non-isothermal atmosphere. The purpose for the derivation of this model is primarily to make a detailed comparison of the theoretically predicted electron density fluctuations with those observed by means of UHF backscatter measurements described in an earlier section. The interaction between the neutral gas wave motion and the plasma is governed by the collisions between the charged and the neutral particles as well as the geomagnetic field which constrains the motion of the charged particles. In the region above about 150 km both the ion-neutral and electron-neutral collision frequencies are much less than the respective gyro-frequencies of the charged particles. Therefore, for motions having periods in excess of the ion-neutral collision time, the only effect of a neutral gas motion is to impart to the ionization its component of velocity along the magnetic field lines. Once the electron velocity field is determined from the neutral gas velocities assuming an appropriate coupling mechanism, the density fluctuations can be derived by solving the electron density continuity equation.

1. Neutral and Electron Gas Velocities

The horizontal and vertical components U_x and U_z of the neutral gas perturbation velocity are expressed in complex Fourier form from wave solutions of the linearized equations of motion, adiabatic state and mass conservation by Hines[1] as:

$$U_x = AX \exp i(\omega t - K_x x - K_z z) \qquad 1(a)$$

$$U_z = AZ \exp i(\omega t - K_x x - K_z z) \qquad 1(b)$$

Various symbols in these and the following equations in this section carry the same meaning as given by Hines, unless otherwise specified. The dispersion equation relating the wave numbers and the frequencies shows that when K_x is real, say $K_x = k_x$, K_z is either purely imaginary or complex. The class of waves which are called internal waves which exhibit both amplitude and phase variations

in vertical direction are of interest in studying the ionospheric disturbances. For the case where the viscous damping of the wave amplitude is ignored, the dispersion relation leads to $K_z = k_z + \frac{i}{2H}$ and

$$U_x = AX \exp \frac{z}{2H} \exp i(\omega t - k_x x - k_z z) \qquad 2(a)$$

$$U_z = AZ \exp \frac{z}{2H} \exp i(\omega t - k_x x - k_z z) \qquad 2(b)$$

where A is a constant and X and Z are the polarization factors given as

$$X = \omega k_x C^2 [k_z - i(1 - \gamma/2) g/C^2] \qquad 3(a)$$

$$Z = \omega^3 - \omega k_x^2 C^2 \qquad 3(b)$$

The wave number k_z, which is real in equations (2) in the absence of viscous damping, would become complex ($k_z = k_z^1$) when the viscous effects are taken into consideration. Pitteway and Hines[11] obtained a dispersion relation considering viscous damping which may be used to determine the complex k_z^1. In the low frequency case such as of interest in the present analysis, some valid approximations in the dispersion relation yield the following relation for k_z^1:

$$k_z^{1\,2} + k_x^2 + \frac{1}{4H^2} = \frac{2 k_x^2 \omega_g^2/\omega^2}{1 + \sqrt{1 - iD}} \qquad (4)$$

where:

$$D = 4\eta k_x^2 \omega_g^2/\omega^3 \qquad (5)$$

D would have to be taken as 2.26 times that given in equation (5) if, as necessary, the effect of thermal conduction is taken into account (Hines, Personal Communication).

On separating the real and imaginary parts in Equation (4) we have

$$k_z^{1\,2} = \left[\frac{2 k_x^2 \omega_g^2}{\omega^2 D} \left(\frac{\sqrt{1 + D^2} - 1}{2} \right)^{1/2} - k_x^2 - \frac{1}{4H^2} \right]$$

$$+ i \left[\frac{2 k_x^2 \omega_g^2}{\omega^2 D} \left\{ \left(\frac{\sqrt{1 + D^2} + 1}{2} \right)^{1/2} - 1 \right\} \right]$$

Denoting the real and imaginary parts in the above equation as 'a' and 'b' respectively we have for k_z^1

$$k_z^1 = \pm \left[\left(\frac{\sqrt{a^2+b^2}+a}{2} \right)^{1/2} + i \left(\frac{\sqrt{a^2+b^2}-a}{2} \right)^{1/2} \right] \qquad (6)$$

The choice of sign for k_z^1 is governed by the requirement that the amplitude of the wave is attenuated progressively in the positive z direction due to viscous damping. The complex k_z^1 which may be expressed as $(k_z - i\chi)$ where k_z and χ are real modifies the perturbation velocity components U_x and U_z as:

$$U_x = AX \exp z \left(\frac{1}{2H} - \chi \right) \exp i (\omega t - k_x x - k_z z) \qquad 7(a)$$

$$U_z = AZ \exp z \left(\frac{1}{2H} - \chi \right) \exp i (\omega t - k_x x - k_z z) \qquad 7(b)$$

The polarization factor X is now modified in that the k_z in equation 3(a) is replaced by k_z^1. Z, however, remains the same as in 3(b). The component of the neutral gas velocity along the geomagnetic field which is effective in driving the plasma can be expressed for the velocity and magnetic field configuration shown in Figure 17 as:

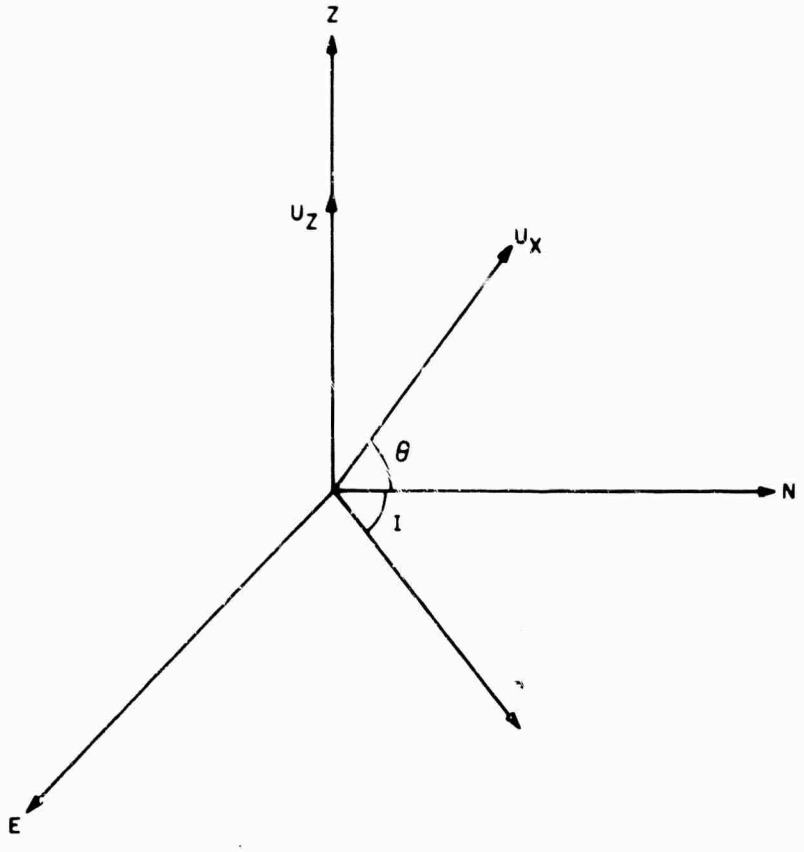

Figure 17. The Neutral Gas Velocity and the Geomagnetic Field Configuration

$$V_B = (U_x \cos\theta \cos I - U_z \sin I)$$

where θ is the angle of direction of U_x measured west of north and I is the magnetic dip angle.

The horizontal and vertical components V_x and V_z of the electron gas in the directions of U_x and U_z are respectively:

$$V_x = V_B \cos I \cos\theta$$

$$V_z = -V_B \sin I$$

Substituting for V_B and then expanding for U_x and U_z we get:

$$V_x = \left[X \cos^2 \theta \cos^2 I - Z \sin I \cos I \cos \theta \right] A \exp z \left(\frac{1}{2H} - \chi \right)$$

$$\exp i (\omega t - k_x x - k_z z) \qquad 8(a)$$

$$V_z = \left[Z \sin^2 I - X \sin I \cos I \cos \theta \right] A \exp z \left(\frac{1}{2H} - \chi \right)$$

$$\exp i (\omega t - k_x x - k_z z) \qquad 8(b)$$

on separating the real and imaginary parts in the amplitude factors the equations 8(a) and 8(b) may be written in the following form:

$$V_x = (P+iQ) A \exp z(\frac{1}{2H} - \chi) \exp i (\omega t - k_x x - k_z z) \qquad 9(a)$$

$$V_z = (R+iS) A \exp z(\frac{1}{2H} - \chi) \exp i (\omega t - k_x x - k_z z) \qquad 9(b)$$

where

$$P = \omega k_x k_z C^2 \cos^2 \theta \cos^2 I - (\omega^3 - \omega k_x^2 C^2) \sin I \cos I \cos \theta$$

$$Q = -\omega k_x [\chi C^2 + (1 - \gamma/2) g] \cos^2 \theta \cos^2 I$$

$$R = (\omega^3 - \omega k_x^2 C^2) \sin^2 I - \omega k_x k_z C^2 \sin I \cos I \cos \theta$$

and

$$S = \omega k_x [\chi C^2 + (1 - \gamma/2) g] \sin I \cos I \cos \theta$$

The velocities V_x and V_z of the electrons can now be used to calculate the electron density perturbations from the continuity equation for the electron density.

2. Continuity Equation

The continuity equation for both electrons and ions in the ionosphere where their densities are assumed to be equal may be expressed in the form:

$$\frac{\partial N}{\partial t} + \nabla \cdot [N (V_d + V_e)] = Q - L \qquad (10)$$

where Q and L are the production and loss rates

N = electron (or ion) density
V_d = diffusion velocity of the ionization
V_e = drift velocity due to electric fields

L has the form of βN in the F region and αN^2 in the E region.

In the present analysis L is represented by βN by adopting an equivalent for β for the heights below about 180 km where the loss is not of purely attachment-like.

The electron density N is perturbed under the influence of an acoustic gravity wave so that the perturbed density N^1 may be written as:

$$N^1(z) = N(z) + n(z) = N(z) + n_0(z)\, e^{i(\omega t - k_x x - k_z z)} \qquad (11)$$

The continuity equation for the perturbed ionosphere may be written as:

$$\frac{\partial N^1}{\partial t} + \nabla \cdot [N^1 (V + V_d + V_e)] = Q - \beta N^1 \qquad (12)$$

where V is the wave induced velocity of the ionization. Subtracting equation (10) from (12) we have the following equation for density perturbation n.

$$\frac{\partial n}{\partial t} + \nabla \cdot [N^1 V + n (V_d + V_e)] = -\beta n \qquad (13)$$

Assuming that the density perturbation n is much smaller than the ambient electron density N and also the contribution due to diffusion and the electric fields is unimportant for the wave periods of interest,[12, 13] the above equation is simplified to:

$$\frac{\partial n}{\partial t} + \beta n = -\nabla \cdot (NV) \qquad (14)$$

Neglecting the horizontal gradients in the ambient electron density and expanding various terms of equation (14) we have:

$$n(\beta + i\omega) = -N\left[\frac{\partial V_x}{\partial x} + \frac{\partial V_z}{\partial z}\right] - V_z \frac{\partial N}{\partial z}$$

$$\frac{\partial V_x}{\partial x} = -ik_x V_x; \quad \frac{\partial V_z}{\partial z} = \left(\frac{1}{2H} - \chi - ik_z\right) V_z$$

$$n\left[\beta + i\omega\right] = V_x\left[iNk_x\right] + V_z\left[N(\chi - \frac{1}{2H} + i k_z) - \frac{\partial N}{\partial z}\right]$$

$$= A \exp z \left(\frac{1}{2H} - \chi\right) \exp i (\omega t - k_x x - k_z z)$$

$$\left\{(P + iQ)\, iNk_x + (R+iS)\left[N(\chi - \frac{1}{2H} + ik_z) - \frac{\partial N}{\partial z}\right]\right\}$$

$$= A \exp z \left(\frac{1}{2H} - \chi\right) \exp i(\omega t - k_x x - k_z z)\,[f + i\ell]$$

where

$$f = N\left[R\chi - \frac{R}{2H} - Q k_x - Sk_z\right] - R\left(\frac{\partial N}{\partial z}\right)$$

$$\ell = N\left[Pk_x + Rk_z + S\chi - \frac{S}{2H}\right] - S\left(\frac{\partial N}{\partial z}\right)$$

$$n = A \exp z \left(\frac{1}{2H} - \chi\right) \exp i(\omega t - k_x x - k_z z) \frac{[(f\beta + \ell\omega) + i(\ell\beta - f\omega)]}{(\beta^2 + \omega^2)} \qquad (15)$$

The above equation can be used to compute the electron density perturbation n as function of height and time at any given location knowing the following information:

1. The wave parameters ω and k_x (k_z may be computed)
2. A model for the ambient electron density N(z, t)
3. An atmospheric model to calculate H, χ and various other parameters needed for f and g.
4. A model for the loss coefficient $\beta(z)$, and
5. The constant A.

A computer program to calculate the electron density perturbation n(z, t) is being developed with the observed HF and UHF data providing the wave parameters and the ambient electron density model. An atmospheric model appropriate to the period of observation is selected from CIRA (1965). For the attachment coefficient $\beta(z)$, a model originally suggested by Ratcliffe et al [14] and used extensively in later studies will be adopted here. The constant A will be determined by stating the initial value for the perturbation which would be provided from the observations. It is now required that the density perturbation be extracted from the observations for a comparison with the theory. The incoherent backscatter measurements furnish the wave perturbed electron density profiles $N^1(z, t)$. The wave perturbation in the observations is averaged out by performing the running averages of $N^1(z, t)$ with a time scale equal to the predominant wave period which leads to the ambient electron density profiles N(z, t). The difference of $N^1(z, t)$ and N(z, t) gives the perturbation profiles n(z, t).

REFERENCES

1. Hines, C.O., "Internal Atmospheric Gravity Waves at Ionospheric Heights," Can. J. Phys., 38, 1441, 1960.

2. Munro, G.H., "Travelling Ionospheric Disturbances in the F Region," Aust. J. Phys., 11, 91, 1958.

3. Thome, G.D., "Incoherent Scatter Observations of Travelling Ionospheric Disturbances," J. Geophys. Res., 4047, 1964.

4. Hines, C.O., "Atmospheric Gravity Waves High in the Ionosphere," USNC-URSI Spring Meeting, 1965.

5. Munro, G.H., "Travelling Disturbances in the Ionosphere," Proc. Roy. Soc. (London), Ser. A, 202, 208, 1950.

6. Munro, G.H., "Reflections from Irregularities in the Ionosphere," Proc. Roy. Soc. (London), Ser. A, 21[illegible], 447, 1953.

7. Davies, K., and D.M. Baker, "On Frequency Variations of Ionospherically Propagated HF Radio Signals," Radio Science 1, (New Series), No. 5, 545, 1966.

8. Briggs, [illegible] H., G.D. Phillips, and D.H. Shinn, "The Analysis of Observations on Spaced Receivers of the Fading of Radio Signals," Proc. Phys. Soc., London, B68, 481, 1955.

9. Phillips, G.J., and M. Spencer, "The Effects of Anisometric Amplitude Patterns in the Measurement of the Ionospheric Drifts," Proc. Phys. Soc., London, B68, 481, 1955.

10. Budden, K.G., "Radio Waves in the Ionosphere," Cambridge University Press, 1961.

11. Pitteway, M.L.V., and C.O. Hines, "The Viscous Damping of Atmospheric Gravity Waves," Can. J. Phys., 41, 1935, 1963.

12. Cunnold, D.M., "F Region Ionization Perturbations Produced by Transport Effects Associated with Acoustic Gravity Waves," Sylvania Electronic Systems Research Report No. 55[illegible], Waltham, Massachusetts, 1967.

13. Georges, T.M., "Ionospheric Effects of Atmospheric Waves," ESSA Technical Report, Boulder, Colorado, 1967.

14. Ratcliffe, J.A., Schmerling, E.R., C.S.G.K. Setty and J.O. Thomas, "The Rates of Production and Loss of Electrons in the F Region of the Ionosphere," Phil. Trans. Roy. Soc., London, A, 248, 621, 1956.

ACKNOWLEDGEMENTS

It is a pleasure to acknowledge with thanks, the cooperation received from Prof. F. D. Drake and the staff of the Arecibo Ionospheric Observatory in conducting the series of experiments reported here. The authors wish to thank Mr. L. C. Edwards and Mr. F. R. Roberts for constant advise and encouragement throughout the progress of this work. Thanks are also due to Mr. Joe Molla for equipment installation and supervision and Mr. Ned Fenstermacher for data processing.

The Arecibo Ionospheric Cbservatory is operated by Cornell University with the support of the Advanced Research Projects Agency under a research contract with the Air Force office of Scientific Research.

Security Classification

DOCUMENT CONTROL DATA - R&D

(Security classification of title, body of abstract and indexing annotation must be entered when the overall report is classified)

1 ORIGINATING ACTIVITY *(Corporate author)*
Raytheon Company, Spencer Laboratory
Burlington, Massachusetts

2a REPORT SECURITY CLASSIFICATION
Unclassified

2b GROUP

3 REPORT TITLE
AN EXPERIMENTAL TEST OF THE ACOUSTIC-GRAVITY WAVE INTERPRETATION OF TRAVELLING IONOSPHERIC DISTURBANCES

4 DESCRIPTIVE NOTES *(Type of report and inclusive dates)*
Interim Scientific Report. 1 April 1967 through 31 March 1968

5 AUTHOR(S) *(Last name, first name, initial)*
Thome, George D.
Rao, Pendyala B.

6 REPORT DATE	7a TOTAL NO OF PAGES	7b NO OF REFS
May 1968	42	14

8a CONTRACT OR GRANT NO	9a ORIGINATOR'S REPORT NUMBER(S)
DA-01-021-1448 Z)	
b PROJECT NO 5910-21-10039-02	INTERIM
c	9b OTHER REPORT NO(S) *(Any other numbers that may be assigned this report)*
d	

10 AVAILABILITY/LIMITATION NOTICES
Agencies of the Department of Defense, their contractors, and other Government agencies may request copies directly from DDC. All other persons and organizations should apply to the Clearinghouse for Federal Scientific and Technical Information (CFSTI), Sills Building, 5285 Port Royal Road, Springfield, Virginia 22151.

11 SUPPLEMENTARY NOTES

12 SPONSORING MILITARY ACTIVITY
Advanced Research Projects - Agency
Washington, D. C.

13 ABSTRACT

This report presents the results of simultaneous HF Doppler and UHF incoherent backscatter measurements of the travelling ionospheric disturbances observed at Arecibo (P.R.) during the summer of 1967. One of the prime objectives in conducting this series of experiments involving 3 spaced phase path sounders and the backscatter radar is to examine the gravity wave interpretation of the large scale travelling disturbances. The analysis of the observations is based upon three distinct techniques: (1) Cross-correlation analysis of the HF Doppler records for an accurate estimate of the wave velocity, (2) HF ray tracing for demonstrating the self-consistency of the HF and the incoherent backscatter data, and (3) the coupling of acoustic gravity waves to the ionospheric plasma. It is concluded from the results of the analysis that the large scale travelling ionospheric disturbances are truly a manifestation of the acoustic-gravity waves. Finally, some aspects of the analysis which will be refined in the next phase of the study are also outlined.

DD FORM 1 JAN 64 1473

Security Classification

14 KEY WORDS	LINK A		LINK B		LINK C	
	ROLE	WT	ROLE	WT	ROLE	WT
Travelling Ionospheric disturbance						
Incoherent backscatter						
Phase Path						
Doppler Shift						
Acoustic-gravity wave						
Ray Tracing						
Cross Correlation						
Wave interaction						

INSTRUCTIONS

1. ORIGINATING ACTIVITY. Enter the name and address of the contractor, subcontractor, grantee, Department of Defense activity or other organization *(corporate author)* issuing the report.

2*a*. REPORT SECURITY CLASSIFICATION: Enter the overall security classification of the report. Indicate whether "Restricted Data" is included. Marking is to be in accordance with appropriate security regulations.

2*b*. GROUP: Automatic downgrading is specified in DoD Directive 5200.10 and Armed Forces Industrial Manual. Enter the group number. Also, when applicable, show that optional markings have been used for Group 3 and Group 4 as authorized.

3. REPORT TITLE: Enter the complete report title in all capital letters. Titles in all cases should be unclassified. If a meaningful title cannot be selected without classification, show title classification in all capitals in parenthesis immediately following the title.

4. DESCRIPTIVE NOTES: If appropriate, enter the type of report, e.g., interim, progress, summary, annual, or final. Give the inclusive dates when a specific reporting period is covered.

5. AUTHOR(S): Enter the name(s) of author(s) as shown on or in the report. Enter last name, first name, middle initial. If military, show rank and branch of service. The name of the principal author is an absolute minimum requirement.

6. REPORT DATE: Enter the date of the report as day, month, year, or month, year. If more than one date appears on the report, use date of publication.

7*a*. TOTAL NUMBER OF PAGES: The total page count should follow normal pagination procedures, i.e., enter the number of pages containing information.

7*b*. NUMBER OF REFERENCES: Enter the total number of references cited in the report.

8*a*. CONTRACT OR GRANT NUMBER: If appropriate, enter the applicable number of the contract or grant under which the report was written.

8*b*, 8*c*, & 8*d*. PROJECT NUMBER: Enter the appropriate military department identification, such as project number, subproject number, system numbers, task number, etc.

9*a*. ORIGINATOR'S REPORT NUMBER(S): Enter the official report number by which the document will be identified and controlled by the originating activity. This number must be unique to this report.

9*b*. OTHER REPORT NUMBER(S): If the report has been assigned any other report numbers *(either by the originator or by the sponsor)*, also enter this number(s).

10. AVAILABILITY/LIMITATION NOTICES: Enter any limitations on further dissemination of the report, other than those imposed by security classification, using standard statements such as:

(1) "Qualified requesters may obtain copies of this report from DDC."

(2) "Foreign announcement and dissemination of this report by DDC is not authorized."

(3) "U. S. Government agencies may obtain copies of this report directly from DDC. Other qualified DDC users shall request through _____."

(4) "U. S. military agencies may obtain copies of this report directly from DDC. Other qualified users shall request through _____."

(5) "All distribution of this report is controlled. Qualified DDC users shall request through _____."

If the report has been furnished to the Office of Technical Services, Department of Commerce, for sale to the public, indicate this fact and enter the price, if known.

11. SUPPLEMENTARY NOTES: Use for additional explanatory notes.

12. SPONSORING MILITARY ACTIVITY: Enter the name of the departmental project office or laboratory sponsoring *(paying for)* the research and development. Include address.

13 ABSTRACT: Enter an abstract giving a brief and factual summary of the document indicative of the report, even though it may also appear elsewhere in the body of the technical report. If additional space is required, a continuation sheet shall be attached.

It is highly desirable that the abstract of classified reports be unclassified. Each paragraph of the abstract shall end with an indication of the military security classification of the information in the paragraph, represented as *(TS)*, *(S)*, *(C)*, or *(U)*.

There is no limitation on the length of the abstract. However, the suggested length is from 150 to 225 words.

14. KEY WORDS: Key words are technically meaningful terms or short phrases that characterize a report and may be used as index entries for cataloging the report. Key words must be selected so that no security classification is required. Identifiers, such as equipment model designation, trade name, military project code name, geographic location, may be used as key words but will be followed by an indication of technical context. The assignment of links, rules, and weights is optional.